Reviews of Geophysics

REVIEW ARTICLE
10.1029/2019RG000651

GRAND CHALLENGES CENTENNIAL COLLECTION

Major Ice Sheet Change in the Weddell Sea Sector of West Antarctica Over the Last 5,000 Years

Martin J. Siegert[1], Jonathan Kingslake[2], Neil Ross[3], Pippa L. Whitehouse[4], John Woodward[5], Stewart S. R. Jamieson[4], Michael J. Bentley[4], Kate Winter[5], Martin Wearing[2], Andrew S. Hein[6], Hafeez Jeofry[1], and David E. Sugden[6]

[1]Grantham Institute and Department of Earth Science and Engineering, Imperial College London, London, UK, [2]Lamont-Doherty Earth Observatory, Columbia University, Palisades, NY, USA, [3]School of Geography, Politics and Sociology, Newcastle University, Newcastle, UK, [4]Department of Geography, Durham University, Durham, UK, [5]Department of Geography and Environmental Sciences, Faculty of Engineering and Environment, Northumbria University, Newcastle, UK, [6]School of GeoSciences, University of Edinburgh, Edinburgh, UK

Key Points:
- The Weddell Sector has experienced major change since the Late Holocene
- It is unclear whether the ice sheet gradually shrank to its modern size from its full-glacial state or became smaller here and then regrew
- Targeted geophysical dating of buried and exposed surfaces and sediment drilling may resolve the inconsistencies in glacial history

Correspondence to:
M. J. Siegert,
m.siegert@imperial.ac.uk

Citation:
Siegert, M. J., Kingslake, J., Ross, N., Whitehouse, P. L., Woodward, J., Jamieson, S. S. R., et al. (2019). Major ice sheet change in the Weddell Sea Sector of West Antarctica over the last 5,000 years. *Reviews of Geophysics*, *57*, 1197–1223. https://doi.org/10.1029/2019RG000651

Received 23 APR 2019
Accepted 11 AUG 2019
Accepted article online 3 SEP 2019
Published online 6 NOV 2019

Abstract Until recently, little was known about the Weddell Sea sector of the West Antarctic Ice Sheet. In the last 10 years, a variety of expeditions and numerical modelling experiments have improved knowledge of its glaciology, glacial geology and tectonic setting. Two of the sector's largest ice streams rest on a steep reverse-sloping bed yet, despite being vulnerable to change, satellite observations show contemporary stability. There is clear evidence for major ice sheet reconfiguration in the last few thousand years, however. Knowing precisely how and when the ice sheet has changed in the past would allow us to better understand whether it is now at risk. Two competing hypotheses have been established for this glacial history. In one, the ice sheet retreated and thinned progressively from its Last Glacial Maximum position. Retreat stopped at, or very near, the present position in the Late Holocene. Alternatively, in the Late Holocene, the ice sheet retreated significantly upstream of its present grounding line and then advanced to today's location due to glacial isostatic adjustment and ice shelf and ice rise buttressing. Both hypotheses point to data and theory in their support yet neither has been unequivocally tested or falsified. Here we review geophysical evidence to determine how each hypothesis has been formed, where there are inconsistencies in the respective glacial histories, how they may be tested or reconciled, and what new evidence is required to reach a common model for the Late Holocene ice sheet history of the Weddell Sea sector of West Antarctica.

Plain Language Summary The West Antarctic Ice Sheet is vulnerable to climate and ocean warming because it rests on a bed more than 2 km below sea level in some places. Understanding how this ice sheet has changed in the recent past guides our appreciation of how it will change in the near future. Getting such information requires measurement of (1) structures in the ice that reflect former ice sheet change; (2) the age when rock surfaces were most recently exposed or covered by ice; and (3) computer calculations of ice sheet processes to understand what change is realistic. The ice sheet was certainly a lot bigger during the ice age, about 20,000 years ago, but two alternative histories exist on how it shrank to today's size in the last 5,000 years. In one, the ice sheet gets smaller gradually over time, and in the other the ice sheet becomes smaller than today before it expands to its current position. Arriving at a single history for the ice sheet may allow us to better understand whether to expect change to occur here in future and how it may happen.

1. Introduction

Quantification of future sea level rise is hindered by uncertainty regarding how the world's polar ice sheets will change under global warming scenarios (Intergovernmental Panel on Climate Change, 2013). While satellite observations have allowed an appreciation of how ice sheets are changing today (and over the last 40 years; Shepherd, 2018; Rignot et al., 2018) key to understanding how they will change in the future is knowledge of their most recent significant alterations. However, this knowledge requires that we have proficient geophysical measurements of ice sheet form and flow, and of past change, in the most vulnerable ice sheet regions.

The Weddell Sea (WS) sector of the West Antarctic Ice Sheet (WAIS; Figure 1) was, until 10 years ago, one of the poorest understood regions of Antarctica. Since then there has been a plethora of airborne and ground

based geophysics (including ice-penetrating radar and solid Earth measurements), glacial geological and geomorphological analyses (including cosmogenic nuclide dating of exposed surfaces), and numerical modelling activities (of ice and Earth). An area of focus for research within the WS sector has been the Southern WS embayment (SWSE), including the Rutford, Institute, Möller, and Foundation ice streams (RIS, IIS, MIS and FIS) and the Bungenstock, Henry, and Korff ice rises (BIR, HIR, and KIR). Investigations here point to substantial change to this sector of the WAIS during the Holocene. However, the details of this change are open to debate, with some considering progressive monotonic retreat of the ice sheet margin from a Last Glacial Maximum (LGM) position at the edge of the continental shelf, with associated ice flow reconfiguration (Hillenbrand et al., 2014), and others suggesting the grounding line retreated significantly inland of its present position, with subsequent ice sheet readvance and flow reconfiguration (Bradley et al., 2015; Kingslake et al., 2018; Siegert et al., 2013). There is also a lack of consensus on the timing of this change, due to a shortage of absolute dating controls and, presently, no synthesis of the ideas published. Here, by reviewing the available information, we establish how each of the glacial histories are supported with data and models, where evidence is contradictory, and what new data might be needed to reach a single consistent glacial history for the region. This is important, because the SWSE could be at a physical threshold of major change, with two ice streams sitting atop a major reversing bed slope, and several ice streams grounded far (~2 km) below sea level (Jeofry, Ross, Corr et al., 2018; Ross et al., 2012). This makes them potentially unstable to perturbations in grounding line position (Wright et al., 2014). Conversely, three large ice rises and a set of ice rumples (slow-moving regions of grounded ice) sit within the Ronne Filchner Ice Shelf (RFIS), providing pinning points for ice-shelf buttressing to these ice streams, which tends to stabilize grounding lines (Matsuoka et al., 2015). By understanding past ice sheet change in this region, in particular assessing whether the ice sheet has retreated or expanded recently in the Holocene and if it is currently experiencing ongoing change, we can better evaluate how the ice sheet may change in the future.

The recent literature has been developed as a consequence of several geophysical campaigns and techniques. It has benefitted from airborne and ground- based ice-penetrating radar, solid Earth lithospheric measurements, cosmogenic nuclide analysis, and numerical ice sheet and solid Earth modelling. This review thus draws together a variety of geophysical techniques and integrates and evaluates the data from these techniques to understand the glacial history of this enigmatic region of West Antarctica, during the Holocene.

2. The Southern Weddell Sea Embayment of the WAIS

The SWSE was the subject of a major aerogeophysical survey in 2010–2011 (Ross et al., 2012), revealing the ~2-km-deep Robin Subglacial Basin immediately upstream of present-day grounding lines. The revised bed was used in ice sheet modelling to quantify the sensitivity of this part of the ice sheet to ocean and atmospheric forcing (Wright et al., 2014). Further geophysical surveying of the region, both by air and on ice, has been undertaken since Bedmap2 (Fretwell et al., 2013) by the British Antarctic Survey (Rosier et al., 2018; Winter et al., 2018) and NASA's Operation IceBridge (operated by the CReSIS and the University of Kansas, https://www.cresis.ku.edu/). This has improved our knowledge of the land surface beneath the ice sheet, leading to a revised digital bed elevation model (DEM) of the region (Jeofry, Ross, Corr, et al., 2018). Immediately to the north of the region targeted by these studies, two ground-based geophysics traverses of the southern RFIS and several of the region's ice rises were conducted in 2013–2015, also by the British Antarctic Survey (Kingslake et al., 2016).

2.1. Geology and Topography

Geophysical data reveal that the WS sector encompasses thinned crust extending ~1,200 km from the continental slope to the Ellsworth-Whitmore Mountains tectonic block (Jordan et al., 2013). The Ellsworth-Whitmore Mountains tectonic block (Dalziel & Elliot, 1982) is bounded on its north side by the WS embayment and the Antarctic Peninsula. IIS and MIS flow north from the block into the RFIS. Several isolated nunataks (e.g., Pirrit Hills, Martin-Nash Hills and Pagano Nunatak) that protrude above the ice surface across the WS sector, result from a ~5- to 10-km-thick Jurassic granite intrusion dated to ~175 Ma (Jordan et al., 2013). The Pagano Shear Zone is a major crustal shear boundary with a dominant NW-SE trend (Curtis, 2001; Jordan et al., 2013). It is located across the region of the Transitional and

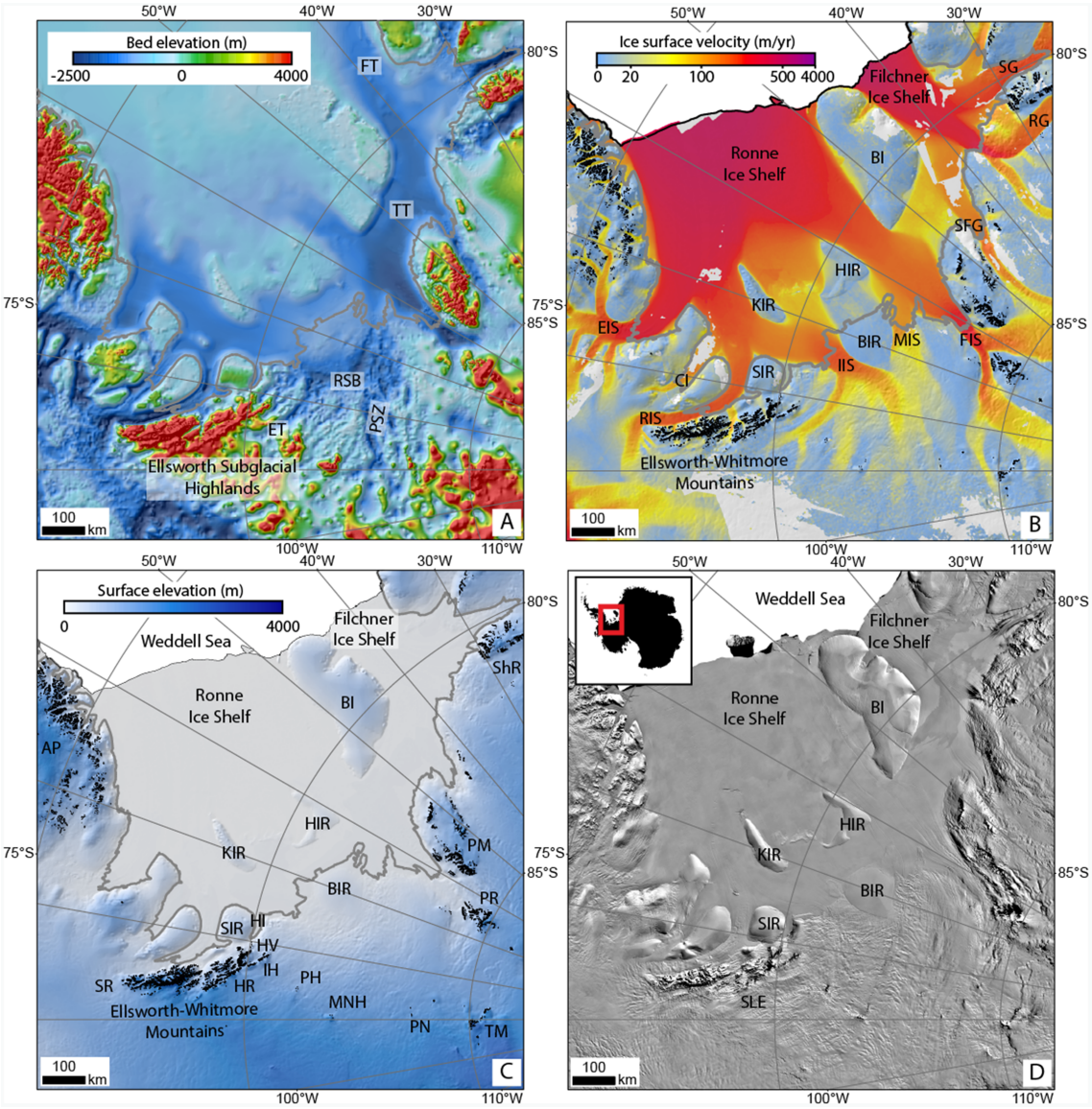

Figure 1. Ice and bed characteristics of the Weddell Sea region. (a) Bed elevation (Fretwell et al., 2013); (b) Ice velocity (Rignot et al., 2011); and (c) Ice surface elevation (Fretwell et al., 2013). (d) MODIS ice surface morphology (Haran et al., 2005; Scambos et al., 2007). The modern grounding line (Haran et al., 2005) is shown as a grey line in a–c and the locations of ice-free regions (black areas) are shown in b and c; Inset shows figure location. RSB = Robin Subglacial Basin; AP = Antarctic Peninsula; IIS = Institute Ice Stream; MIS = Möller Ice Stream; FIS = Foundation Ice Stream; RIS = Rutford Ice Stream; SFG = Support Force Glacier; RG = Recovery Glacier; SG = Slessor Glacier; CI = Carson Inlet Glacier; BIR = Bungenstock Ice Rise; BI = Berkener Island; HIR = Henry Ice Rise; KIR = Korf Ice Rise; SIR = Skytrain Ice Rise; PH = Pirrit Hills; MNH = Martin-Nash Hills; PN = Pagano Nunatak; PSZ = Pagano Shear Zone; HV = Horseshoe Valley; IH = Independence Hills; PM = Pensacola Mountains; PR = Patuxent Range; ShR = Shackleton Range; TM = Thiel Mountains; ET = Ellsworth Trough; HR = Heritage Range; SR = Sentinel Range; FT = Filchner Trough; TT = Thiel Trough; SLE = Lake Ellsworth; HI = Hercules Inlet.

Marginal Basins, where it is overlain with highly deformed Palaeozoic metasediments (512–250 Ma). Aeromagnetic anomalies indicate that Palaeozoic metasediments and ~13-km-thick Cambrian igneous rocks overlie the Proterozoic basement (2,500–541 Ma) in several sectors of the Ellsworth domain (Jordan et al., 2013).

The bed topography of the WS sector is both rough (over mountains and exposed bedrock) and smooth (e.g., across sediment-filled regions; Bingham & Siegert, 2007). The deepest parts of the Robin Subglacial Basin (Figure 1a) are anomalously rough, marking the edge of a sedimentary drape (Siegert et al., 2016), while the subglacial topography of the region between the Robin Subglacial Basin and the Pirrit and Martin-Nash Hills is relatively flat, smooth, and gently sloping. Rose et al. (2015) defined this flat region as a

bedrock planation surface: a geomorphological feature that might be attributable by marine and/or fluvial erosion (Sugden & Jamieson, 2018). A series of large subparallel subglacial bed channels, thought to have been formed by the flow of basal water, lie between the MIS and FIS (Figure 1b; Rose et al., 2014). As these channels are presently located beneath slow moving and cold-based ice, the channels must be ancient, possibly formed at a time when the ice sheet was warm-based in this region and surface melting was prevalent in West Antarctica. Field evidence and modelling suggests that such conditions may have last existed in the mid-Miocene (Sugden et al., 2017). In other parts of the WS sector higher bed elevations allow the RFIS to ground, creating ice surface features known as ice rises and rumples (Matsuoka et al., 2015), the largest of which include the BIR and HIR (Figure 1).

2.2. Glaciology

The SWSE is composed of three major ice sheet outlets (Figure 1): the IIS, MIS, and FIS, respectively, feeding ice to the Ronne-Filchner Ice Shelf, the second largest ice shelf in Antarctica after the Ross Ice Shelf. Subglacial topography and geology control the position and dynamics of these ice streams. (The downstream ice shelf is also a major control on dynamics and grounding line position.) The IIS and MIS grounding lines sit atop a steep reverse bed slope (Ross et al., 2012), similar in scale to that measured for upstream Thwaites Glacier. The bed slopes inland to a ~2-km-deep basin (the Robin Subglacial Basin), which is divided into two sections, with few obvious significant ice sheet pinning points (Ross et al., 2012).

The IIS has three tributaries to the south and west of the Ellsworth Mountains, occupying the Horseshoe Valley, Independence Trough, and Ellsworth Trough (Bamber et al., 2000; Ross et al., 2014; Winter et al., 2015). The Horseshoe Valley trough, around 20-km wide and 1.3-km below sea level at its deepest point, is located downstream of the steep mountains of the Heritage Range. A subglacial ridge is located between the mouth of the Horseshoe Valley trough and the main trunk of the IIS (Winter et al., 2015). The Independence Trough is subparallel to the Horseshoe Valley trough, separated by the 1.4-km high Independence Hills. The trough is ~22-km wide and over 1-km below sea level at its deepest point. It is characterized by two distinctive plateaus (~6-km wide each) on either side of the trough, which are aligned alongside the main trough axis. Presently, ice flows eastward through the Independence Trough for ~54 km before it shifts to a northward direction, where the trough widens to 50 km at its connection with the main IIS. The Ellsworth Trough (Ross et al., 2014) is aligned with the Independence Trough; both are orthogonal to the orientation of the Amundsen-Weddell ice divide, dissecting the Ellsworth Subglacial Highlands northwest to southeast. The Ellsworth Trough is considered to be the largest and deepest trough-controlled tributary of the IIS (Ross et al., 2014; Winter et al., 2015), measuring ~34 km in width and ~260 km in length. At its deepest point, the Ellsworth Trough extends ~2 km below sea level. The trough contains the ~10- to 15-km-long Ellsworth Subglacial Lake (Siegert et al., 2012; Siegert et al., 2004; Woodward et al., 2010). The Ellsworth Trough is intersected by several smaller valleys aligned perpendicularly to the main axis, which are relic landforms from a past small dynamic ice mass (predating the WAIS in its present configuration; Ross et al., 2014).

The MIS is smaller and slower than IIS and is supplied by ice from the upstream IIS tributary (Mouginot et al., 2017). A bifurcation south of the BIR sends most of the ice into the IIS trunk and a smaller fraction into the MIS. The shear margins of the two ice streams interact differently with the BIR. The IIS-BIR shear margin is controlled thermally; the IIS bed is wet while the BIR is frozen at its base (Siegert et al., 2016). The MIS-BIR margin is controlled tectonically by the Pagano Shear Zone (see below), which has created a subglacial trough, currently occupied by the MIS.

The trunk of the FIS occupies a very deep (~2 km) trench, fed by ice from both the WAIS (via an upstream tributary of the FIS), and the East Antarctic Ice Sheet (through Academy Glacier). The grounding line of the FIS rests on a horizontal bed and has been shown to oscillate across the bed by ~20 km as a consequence of tidal forcing, where the trunk of the ice stream is floated at high tide and grounded at low tide (Jeofry, Ross, Le Brocq et al., 2018).

The flow of subglacial water is critical to the ice dynamics of the WS sector of the WAIS. Jeofry, Ross, Le Brocq, et al. (2018) calculated the pathways of basal water flow using recently constructed bed and surface DEMs. This study reveals how water flows beneath the tributaries and into the trunks of the ice streams. It also shows how each of the ice streams interacts distinctly with this water. For IIS, the greatest surface ice flow velocities are recorded across a well-defined sedimentary drape, which is predominantly fed by

water from the upstream IIS catchment. This water also feeds the Robin Subglacial Basin, where it exits the ice sheet as a point source, etching a channel into the ice shelf above (Le Brocq et al., 2013). This water acts to weaken the sediment, so allowing the fastest ice velocities above it (Siegert et al., 2016). For FIS, significant levels of water are provided by Academy Glacier (i.e., from East Antarctica), in which over a dozen "active" subglacial lakes exist all the way upstream to the South Pole (Wright & Siegert, 2012; Jordan et al., 2018; Smith et al., 2009). Across the floor of the ice stream trunk, flow-parallel hard-rock landforms channel water so that it too exits as a point source, leading to an ice shelf channel >130 km in length (Jeofry, Ross, Le Brocq, et al., 2018).

2.3. Sensitivity of the Region to Future Change

The discovery that the IIS and MIS grounding lines are perched on the top of a major reverse bed slope revealed that they are potentially at a threshold of substantial glaciological change through marine ice sheet instability (Ross et al., 2012). This concern was added to by numerical ocean modelling, which predicted enhanced flow of warm water to the WS grounding lines by the end of this century as a consequence of wind-pattern changes offshore (Hellmer et al., 2012), suggesting the potential for future ice losses from this sector equivalent to ~0.3 m of sea level rise. To investigate the sensitivity of the WS sector ice streams to future ocean-driven warming, Wright et al. (2014) used the BISICLES ice sheet model (which includes appropriate grounding line physics) to determine grounding line dynamics of WS ice streams under ocean warming scenarios, leading to an appreciation of the conditions that deliver grounded ice retreat and an understanding of the regions most sensitive to such change (Figure 2). The model was first run using best estimates of basal ice sheet parameters, ice accumulation and grounding line melt rates. The first "control" experiment ran this model for 2,000 years, with the hope of replicating the present-day ice sheet configuration. However, in this run, the IIS began to lose mass by around 200 years and experienced accelerating mass loss in the subsequent 1,800 years. By the end of the model run, it was losing around 8 km^3 of ice annually. Similarly, MIS lost mass at a rate of 1–2 km^3 per year. This behavior suggests that the two ice streams are not in equilibrium with the imposed forcing fields, so either these fields are wrong or the ice streams are on the brink of major change. However, as Wright et al. (2014) state, the first run should "be viewed solely as a neutral starting point from which to assess the relative sensitivity of the ice streams to change, and not as a prediction."

The model was then used in a series of experiments that adjusted the levels of ice accumulation and basal ice-shelf melting. Approximately, "stable" ice sheet configurations were obtained for runs where basal melting is reduced compared to the reference run, by as much as half the estimated values of today. However, when small increases were applied to the model, the IIS and MIS experienced mass loss and ice sheet retreat (Figure 2). Indeed, in all runs where increased melting was applied these two ice streams lost mass unabated throughout the 2,000 years of the experiment. Other ice streams, such as Rutford Ice Stream and Carlson Inlet, were relatively unaffected in the experiments, suggesting they are insensitive to small levels of increased rates of basal melting. However, when values around 25% more than today's are used in the model, these glaciers also experience mass loss and ice retreat.

Clearly, the model reveals that the IIS and MIS are the most sensitive ice streams in the WS to future ocean-driven change. Indeed, the IIS appears to be the most sensitive of the entire WAIS in this regard [Cornford et al., 2015]. Their retreat is halted when the entire Robin Subglacial Basin is deglaciated, and the bed slope returns to "normal" (as opposed to reverse).

3. LGM Ice Sheet Configuration and LGM to Mid-Holocene Change

Hillenbrand et al. (2014) compiled ice core data (from Berkner Island and EPICA-Dronning Maud Land), marine geophysical measurements of former glacial landforms, marine sediment core information between the ice-shelf margin and the continental-shelf break, and onshore cosmogenic nuclide dating of rock exposures, to assemble two possible scenarios (MAX and MIN) describing the retreat of the WS sector between 20,000 years ago (i.e., the LGM) and 5,000 years ago (the mid-Holocene). The two scenarios were based on different interpretations of dated material and on the style of glaciation.

Scenario MIN (Figure 3) is based largely on the onshore cosmogenic record (Bentley et al., 2010; Le Brocq et al., 2011; Whitehouse, Bentley, & Le Brocq, 2012) and assumes that the oldest marine sediment dates represent minimum ages for post-LGM ice sheet retreat. It also assumes that subglacial landforms on the present-

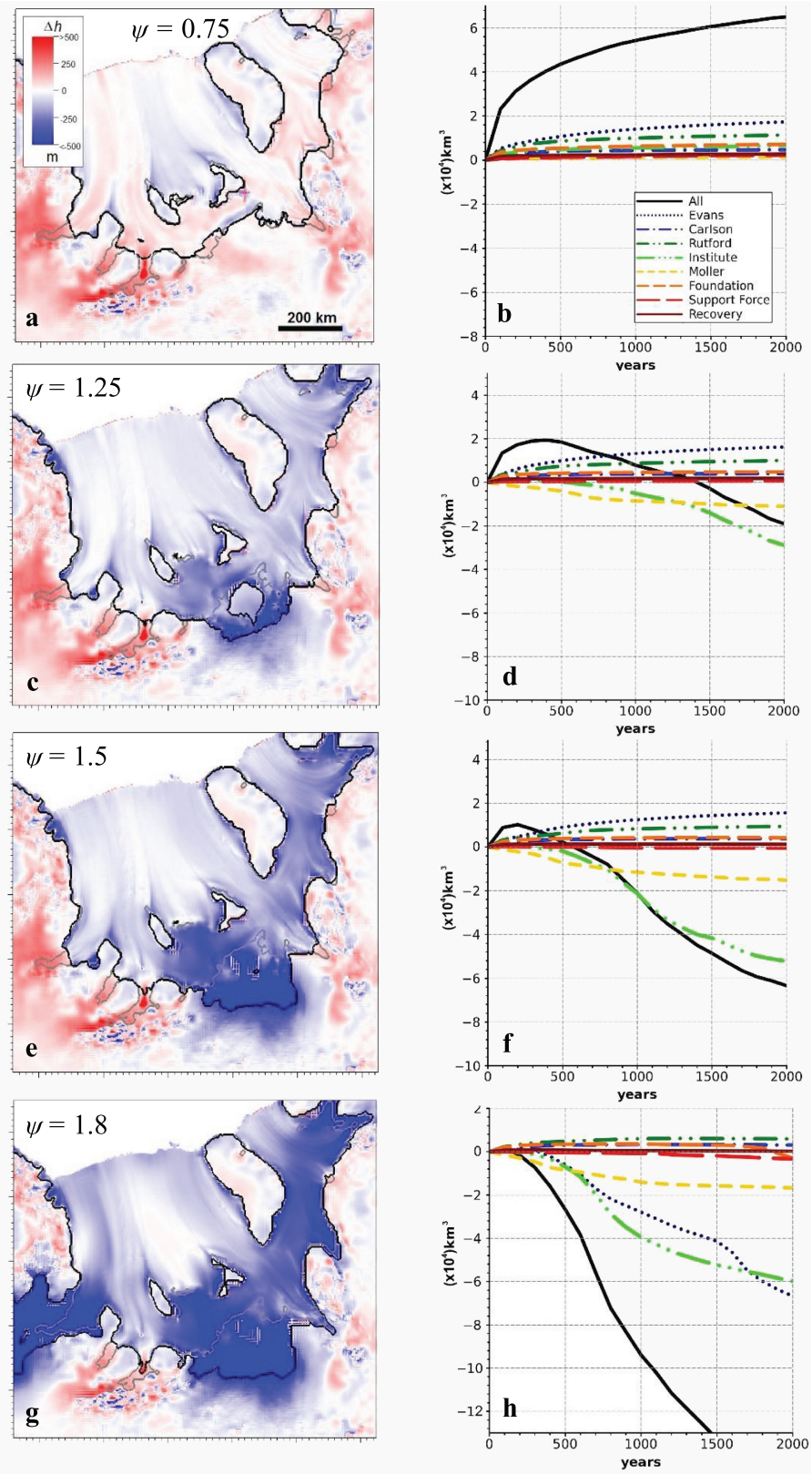

Figure 2. Left hand side (a, c, e, and g) are plan view maps showing changes in ice thickness (color scale) and grounding-line position (grey = start and black = end) over 2,000-year model runs. Right-hand side (b, d, f, and h) are plots of cumulative volume change against time for each of the ice stream catchments for the same experiment. Adapted from Wright et al. (2014).

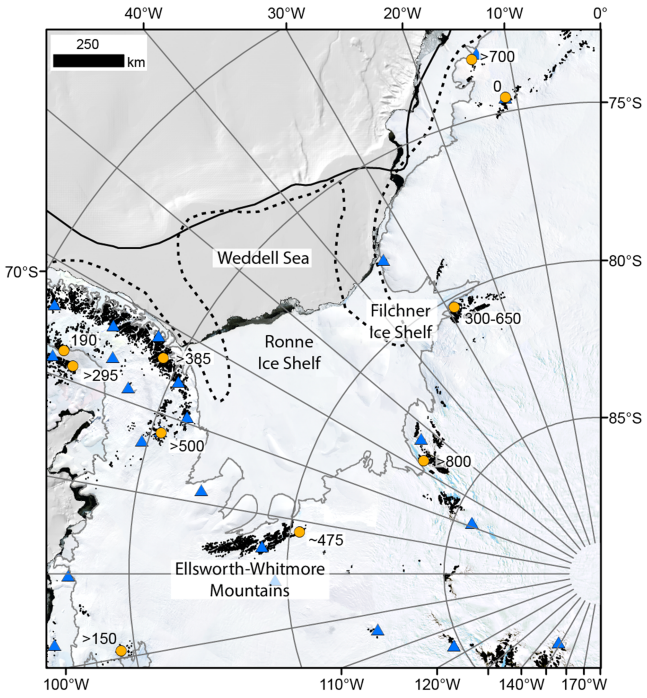

Figure 3. LGM ice extent and thickness change. Solid black line indicates Scenario MAX for LGM ice extent, dashed black line indicates Scenario MIN. Orange points indicate LGM ice thickness (m) difference relative to present (Bentley et al., 2014; Hein, Marrero, et al., 2016; Johnson et al., 2019; Nichols et al., 2019). GPS sites are shown by the blue triangles. Black areas are nunataks; grey line is the modern grounding line. The background is the Landsat Image Mosaic of Antarctica (LIMA) (Bindschadler et al., 2008) in combination with a hill shade of the Weddell Sea bathymetry from Bedmap2 (Fretwell et al., 2013).

day seafloor are pre-LGM in age. Scenario MIN also utilizes an ice sheet model that matches where former ice surface elevation and extent have been constrained using dated onshore exposures. Scenario MAX (Figure 3) assumes that dates from sedimentary cores represent a mixture of maximum and minimum ages for the LGM and its retreat, and that the style of glaciation here was similar to that interpreted elsewhere in Antarctica at the LGM, where ice advanced to the continental shelf break. Scenario MAX requires that the vertical limits of fresh erratics around the WS embayment do not record the LGM limit (Bentley et al., 2011; Clark, 2011) and that the ice was substantially thicker without leaving a detectable geomorphological record. Importantly, both scenarios are consistent with low excess ice volumes during the LGM suggesting the region could only make a minor contribution to global meltwater pulses during the last deglaciation.

Scenario MIN at the LGM involves grounded ice extending across what is now the central RFIS to the continental shelf, and floating ice extending across the channels to the east and west (e.g., the Thiel Trough). At 15,000 years ago, scenario MIN accommodates modest expansion of grounded ice across the continental shelf, where ice sheet extent is limited seaward of the KIR and HIR, and the Thiel Trough is largely free of grounded ice (i.e., modest advance of the FIS). Grounded ice is predicted north of Berkner Island, but absent to the east and west of this lobe. By 10,000 years ago, grounded ice continuously covers the area between the present grounding line and the KIR and HIR. Grounded ice around Berkner Island is more extensive than today but is now cut off from the grounded WAIS. By 5,000 years ago, the WAIS margin was similar to today, Berkner Island still contained more grounded ice than today and the KIR and HIR were joined but separated from the WAIS.

Scenario MAX starts with the grounded ice sheet fully expanded to the continental shelf, with continuous grounded ice across what is now the FRIS. By 15,000 years ago, only modest retreat from this maximum position has occurred, and by 10,000 years, continuous ice cover remains between Berkner Island, the Thiel Trough, and KIR/HIR. By 5,000 years ago, the extent of grounded ice remains substantial; indeed, greater in some places than the LGM configuration in scenario MIN.

4. Radio Echo-Sounding and Englacial Structures

4.1. Background to Radio-Echo Sounding

The two post-LGM scenarios discussed above are obviously in apparent conflict, although both feature a retreat from far out on the continental shelf at the LGM back toward the present-day configuration (Hillenbrand et al., 2014). Our review now concentrates on reconstructing the ice sheet history from the mid-Holocene (~5,000 years ago), using a combination of glaciological data derived from glacier-geophysical investigations, with support from cosmogenic data in locations where both are in close proximity. The use of geophysical data from the ice sheet itself is possible and appropriate, as the ice itself is aged up to and older than 5,000 years (accounting for accumulation, vertical deformation, and lateral transport); hence, changes to ice flow conditions around this time are recorded englacially. While we cannot comment on which of the two LGM scenarios are most accurate, we will comment on which of the two 5,000-year reconstructions best fit with these observations.

The prime data set used here is radio-echo sounding (RES), which can be mounted on aircraft or pulled by snowmobile. The RES technique operates through the emission of a radio wave which propagates through air and into the ice sheet and is reflected off any boundaries separating media with differing dielectric properties (Dowdeswell & Evans, 2004; Siegert, 1999). Radio wave reflections can be identified in RES data from the ice surface and the subglacial bed. In this way, information about Antarctic ice thickness, bed conditions,

and the distribution of subglacial water and lakes has been established (Dowdeswell & Evans, 2004). In addition, Antarctic RES data show a number of strong reflections from within the ice sheet. The most widely noticeable of these englacial reflections are known as internal layers (Siegert, 1999).

Because a radio wave reflection will occur at a boundary of dielectric contrast, the origin of internal layers must be a response to dielectric boundaries within the ice sheet column. There are two possible causes of dielectric variation within the ice sheet: (1) ice density and/or fabric changes and (2) chemical properties of ice (see Siegert, 1999). Observations of density variation within ice cores indicate that below about 500 m of ice depth it will be too small to affect significant dielectric boundaries. Thus, an ice density origin for internal layering is only valid for the uppermost layers of the ice. However, variation in the chemistry of ice and crystal fabric can occur throughout the ice column. The most commonly held view is that dielectric variation is best explained by acidic layering within the ice sheet. Acidic layers originate from an aerosol product derived from volcanic eruptions that subsequently precipitates on the ice surface during snowfall. Burial of this snow eventually causes discrete layers of acid-laden ice at depth within the ice sheet. As ice flows within the ice sheet, these acid layers will deform accordingly. This deformation should result in folding of layers but not necessarily cause discontinuities. Thus, internal RES layering below 500 m is expected to be continuous over several tens to hundreds of kilometers within central slow flowing regions of Antarctica (Siegert, 1999). Such internal layers obey the law of superposition and represent isochronous surfaces.

However, where ice flows more quickly, internal layers buckle and become significantly disrupted and discontinuous. The transition between continuous and buckled layers mark shear zones of ice streams or flow over major subglacial obstacles. If ice flow conditions have changed, the record of former ice flow is thus contained within englacial layers but may be advected downstream or overprinted by subsequent accumulation. Hence, internal layer conditions are especially useful in determining ice-flow modifications in the last few thousand years.

Other englacial layers have been established close to the beds of ice sheets. Where englacial stress is enhanced as ice flows around large subglacial obstacles, crystal fabrics can develop, leading to permittivity layers. Fracture and crevassing of the ice at depth may also lead to distinctive changes in dielectric properties. In addition, layers resulting from accretion of ice from the bed, potentially also involving ice fabric development, have been seen in both slow (Bell et al., 2011; Wrona et al., 2018), enhanced (Wolovick et al., 2014) and in transitional (Bons et al., 2016; Ross & Siegert, 2014) regions of the ice sheet. In such cases, basal "accretion" layers mark a boundary between isochronous ice (conformable with the basal layer, not necessarily the bed) and a basal ice unit with few noticeable layers or features.

Further englacial reflectors may result from basal sediment inclusion (Siegert et al., 2013; Winter et al., 2019) and from where ice is, or has been, floating to form basal crevasses (Kingslake et al., 2018; Wearing & Kingslake, 2019). In all cases, interpreting past flow from internal layers requires consideration of how changes in time may affect layer arrangements. This becomes especially challenging where more than one type of change has occurred, leading to secondary episodes of deformation that may be difficult to distinguish. Nonetheless, analysis of internal layers and structures has proven very useful in determining the recent flow history of both the WAIS (Catania et al., 2012; Conway et al., 1999; Holschuh et al., 2018; Martín et al., 2006; Siegert et al., 2004) and EAIS (Bingham et al., 2007).

4.2. Glacial History of the SWSE Sector From Internal Layering and Basal Features

We summarize englacial structures across the SWSE starting from the ice divide, across the transition to fast flowing ice and onto ice shelves and ice rises. The center of the WAIS contains some of the clearest and best-preserved internal layers on the continent (Siegert & Payne, 2004). Two sets of evidence support the idea that the ice-divid position is unlikely to have changed significantly between the LGM and today. First, by calculating former rates of ice accumulation necessary for the measured distribution of isochronous layers in a transect across the ice divide, it seems likely that the spatial pattern of accumulation has been unchanged in the last 20,000 years (Siegert & Payne, 2004). If the ice divide had changed, the modification to the orographic influence on ice accumulation would lead to an accumulation distribution different in the past compared with today, as observed in Taylor (Morse et al., 1998) and Talos (Siegert & Leysinger Vieli, 2007) ice domes. This is not observed across the WAIS, however, indicating ice-divide stability. Second, small folds within internal layers, caused by ice flow across a rough bed, track downstream with ice flow. By tracing

the troughs and peaks of internal layer folds, a pathway of former ice flow can be established, the date of which begins from when the furthest fold from the rough topography was positioned over it. Ross et al. (2011) calculate stability of the WAIS divide based on an assessment of internal layer structures over Lake Ellsworth experiencing no detectable change from the modern ice flow direction. A similar match between layer structures and modern ice flow is found on the WS side of the ice divide (Ross & Siegert, 2014) and in the Siple Coast (Holschuh et al., 2018). Elsewhere on the Siple Coast side of the divide, however, ice flow direction has been shown to vary by around 30° due to ice relaxation and retreat of grounded ice across the Ross Shelf since the LGM (Siegert et al., 2004).

Further downstream, ice flows into the trunk of IIS through multiple subglacial valleys. Winter et al. (2015) analyzed the internal layers within the Independence, Ellsworth, and Horseshoe Valley troughs, concluding that while the pattern of continuous versus disrupted layers is consistent with modern ice flow, supporting little ice flow direction change, evidence exists for former enhanced flow in these tributaries. Horseshoe Valley also contains basal ice structures associated with subglacial hills and pinnacles that are best explained as inclusions of basal sediment (Siegert et al., 2013; Winter et al., 2019). The feature can be tracked downstream to the trunk of IIS, but no internal layers exist within it, preventing further tracking (Figure 4).

The next location to consider is the BIR, adjacent to the IIS and MIS, which contains key glaciological data constraining the Holocene glacial history of the SWSE. Presently, the BIR has only very slow flowing ice. Most stable ice rises that are frozen at their beds have well-established "Raymond arches" beneath their ice divides, which form as a consequence of non-linear variation in ice rheology with strain rate and stable flow over one characteristic time; the time taken to accumulate the full ice thickness (Martín et al., 2009; Raymond, 1983). Ice rises that do not contain Raymond arches are either too young or have experienced ice divide migration. The BIR contains a small Raymond arch beneath its divide, suggesting recent stability, but not long enough for a major arch to develop (Martín et al., 2009). Satellite imagery reveals the BIR to have relic flow stripes across its surface (Figures 5 and 6), indicating the direction of former ice flow was similar to the present flow direction of the adjacent MIS (Siegert et al., 2013). Beneath the surface, radar has measured buckled internal layers under continuous layers, indicative of ice-dynamic processes being suddenly replaced by stagnant flow (Figure 6). One conclusion to be drawn from these two data sets is that past ice flow across the BIR was aligned with the surface stripes at enhanced flow speeds. Flow would have tracked across what is now the trunk of IIS, emanating from the three tributaries the other side of it (i.e., Ellsworth, Independence, and Horseshoe valleys) (Winter et al., 2015). Siegert et al. (2013) used a simple one-dimensional ice compression model and the modern rate of ice accumulation, to estimate the age of the transition between continuous and buckled layers at around 4,000 years ago.

The radar data also show the bed of BIR to be extremely smooth and continuous between it and the IIS trunk. Hence, the shear margin between the IIS and BIR should be controlled by basal hydrology and thermomechanics; on one side, the IIS is wet based and on the other the BIR is cold based (Figure 6). The shear margin between BIR and MIS is tectonically influenced by the Pagano Shear Zone (Jordan et al., 2013) and may represent a more stable border between fast and slow flow. In summary, these data show that the IIS used to once track across the BIR and over what is now its hydrologically controlled shear margin.

Another interesting englacial feature across BIR is an apparent basal layer (Siegert et al., 2013; Figure 6), which looks remarkably similar in appearance to the sediment inclusion observed in Horseshoe Valley (Winter et al., 2019). It can be traced across the entire BIR along a former flow band (i.e., flow stripes). Interpolation upstream (across what is now the IIS trunk) links it to the feature in Horseshoe Valley, though without drilling through the ice and sampling it is not possible to be certain whether this is the same feature. An alternative explanation for the BIR basal feature is that it represents crevasses along a former shear margin, that have been subsequently filled with salt water.

To the north of BIR, adjacent to the ice plain that separates the grounded ice from the ice shelf, englacial folds can be observed, which are consistent with recent localized advance (i.e., 10–20 km) of the grounding line and expansion of the ice rise. Further downstream, embedded within the Ronne Ice Shelf, are the KIR and HIR and the Doake Ice Rumples (Figure 7). Ice rises are independent flow features with ice flow emanating from their center to the grounding line surrounding them. In contrast, at ice rumples, an ice shelf becomes temporarily grounded and slows significantly before becoming afloat at the downstream margin.

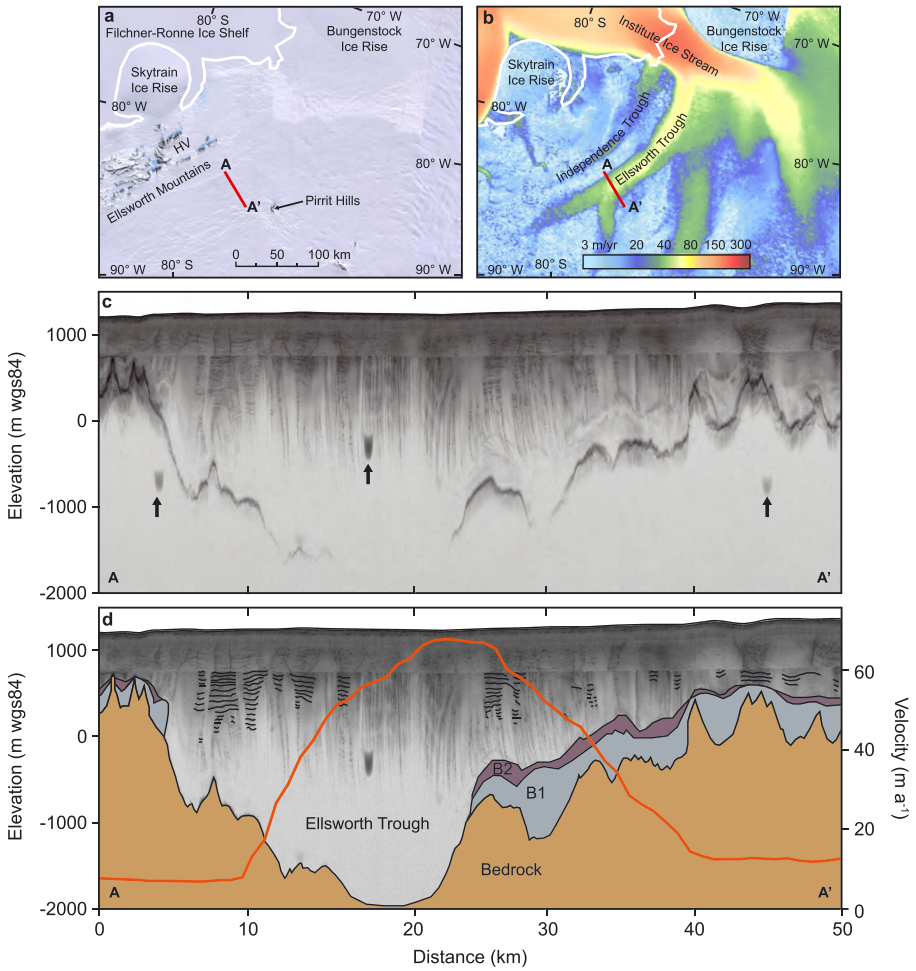

Figure 4. Radar investigations of the Ellsworth Trough. (a) Landsat Image Mosaic of Antarctica (LIMA; Bindschadler et al., 2008) showing surface features, as well as the location of radargram A-A′, which is displayed in (c) and annotated in (d). The white line indicates the ASAID grounding line (Bindschadler et al., 2011). (b) Rignot et al. (2011) MEaSUREs version 2 ice flow map showing enhanced flow speeds in major tributaries of the Institute Ice Stream. (c) SAR-processed radargram across the upper Ellsworth Trough. Arrows indicate processing artefacts, whilst processing steps prevent the upper 200 samples (~500 m) from being imaged. (d) Digitized interpretation of (c), highlighting the basal topography (brown), lower basal ice unit (B1) and upper basal ice unit (B2; as described by Winter et al., 2015) as well as visible englacial stratigraphic layers (black). The secondary axis is the satellite-derived surface ice flow speed from MEaSUREs version 2, shown in the figure as an orange line (Rignot et al., 2011).

The flow of the ice shelf is heavily modified by the presence of the relatively slow-flowing ice rises and rumples. HIR is approximately 100-km northeast of BIR. Ice from the MIS flows pasts its eastern flank, ice from IIS flows past HIR to the west over Doake Ice Rumples, and ice flowing off the front of BIR flows very slowly toward HIR before being diverted westward at HIR's southern flank. KIR lies approximately 200 km to the west of HIR, with ice from IIS flowing past both flanks.

In terms of glaciological setting and planform size, HIR and KIR are similar. Ground-based, 4-MHz RES surveys conducted in 2013/2014 and 2014/2015 showed that they differ significantly in thickness and in englacial structure. KIR consists of a single ice divide, approximately 150-km long, running approximately SW–NE. KIR is approximately 600-m thick at its summit. The bed of KIR is flat and smooth and englacial layers are smooth and conformable everywhere that we have RES data. Beneath the ice divide are prominent Raymond Arches running the length of the ice divide (see Kingslake et al., 2016).

HIR consists of two ridges, each approximately 100-km long, extending to the north and southwest from a peak in surface elevation in the southeast. In contrast to the surface topography, a basal high point is

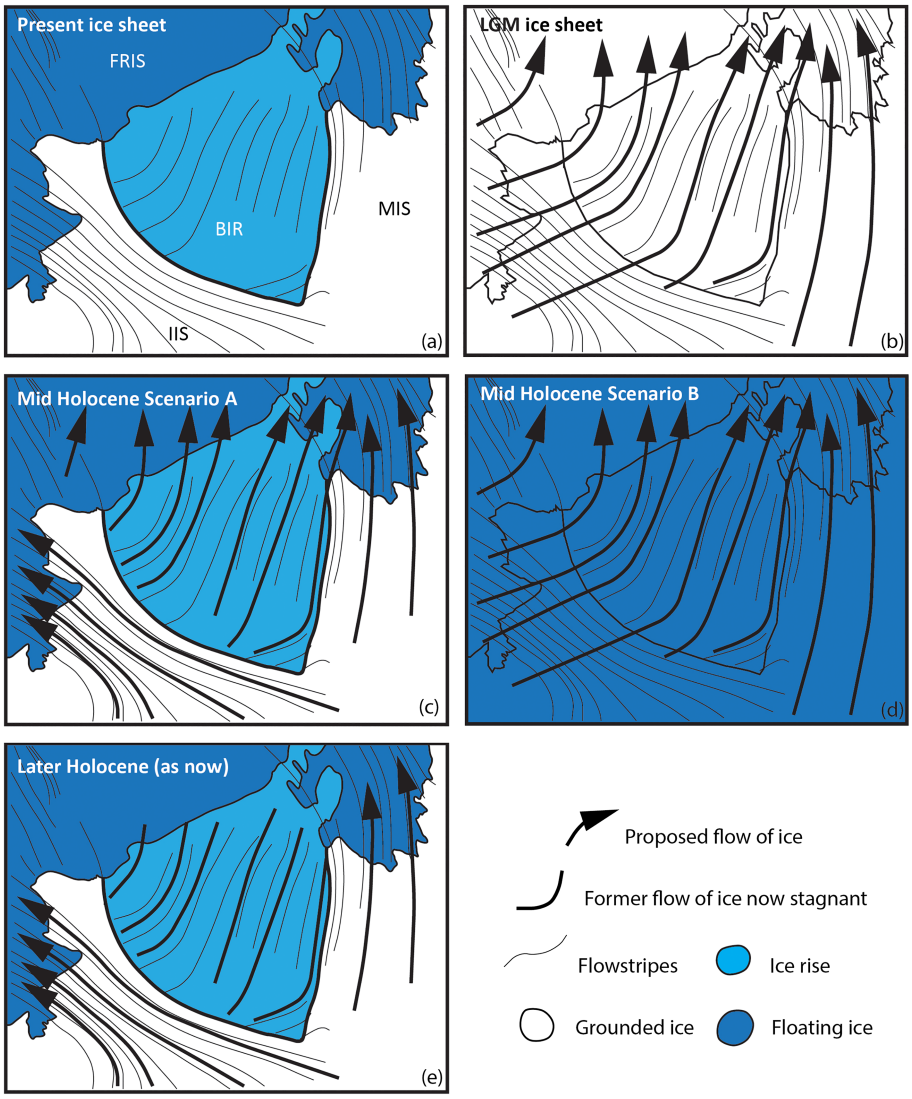

Figure 5. Schematic description of ice sheet change in the BIR region. (a) The current glaciological situation, with ice flow-stripes noted. (b) LGM-type ice sheet, where northward flow of grounded ice from the WAIS interior dominates the region cross cutting the present-day trunk of the IIS and across the BIR. (c) Mid-Holocene Scenario A, where the IIS becomes active to the south of the BIR. (d) Mid-Holocene scenario B, where the grounding line has migrated upstream leaving the BIR region covered by floating ice. (e) Later Holocene ice configuration, in which ice over the BIR becomes stagnant, thus leading to the present-day ice sheet configuration. In the case of a retreat of grounded ice, the IIS activates as a consequence of ice sheet surface lowering and reorganization of the subglacial hydrological regime. In the case of regrounding of the BIR as a consequence of post glacial uplift, the IIS flows along its present direction because of stagnant ice across its northern border. Adapted from Siegert et al. (2013).

located at the northern end of the northern ridge (Wearing & Kingslake, 2019). HIR is 400- to 800-m thick. There are only small, underdeveloped Raymond Arches in HIR, and these are restricted to the northern end of the northern ridge. Elsewhere, Raymond Arches are undetectable. This suggests ice flow has not been stable here for the characteristic time (Martín et al., 2009) of approximately 4.5 kyr (estimated from the radar-derived measured ice thickness and accumulation rates from satellite data (Arthern et al., 2006) and modelling (van Wessem et al., 2018)). From the ground-based RES survey, continuous regions of bright tilted reflectors are observed at the base of HIR up to 12-km inland from the grounding line of the northward pointing promontory (Figure 7). These reflectors are distinct from the ubiquitous internal layers also observed in HIR. Individual dipping reflectors extend vertically 150–200 m into the ice from the base and span up to 2 km horizontally. The isochronal layers intersected by the dipping reflectors

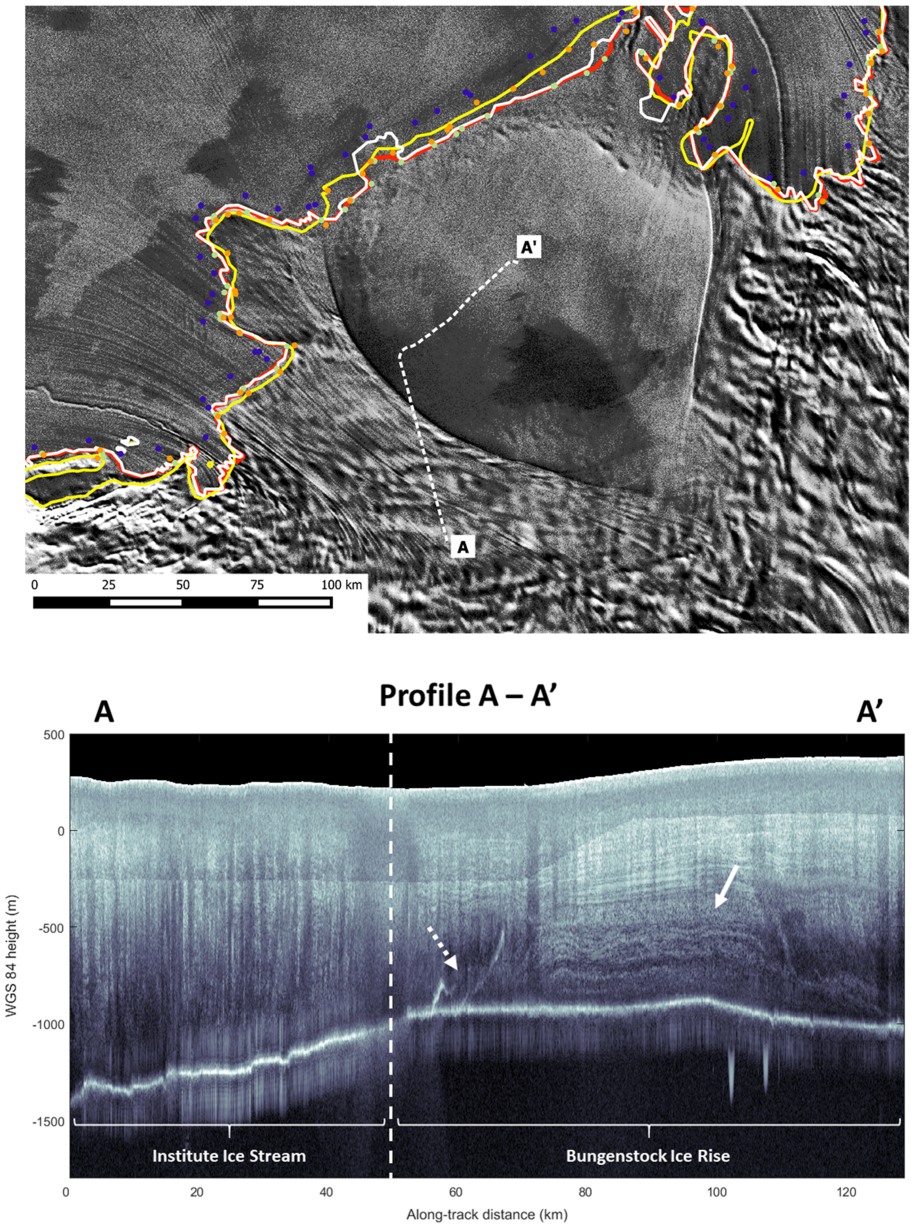

Figure 6. (upper panel) MODIS image of the Bungenstock Ice Rise (BIR), with Institute Ice Stream (IIS) to the south, and Möller Ice Stream (MIS) to the East. Note the palaeosurface flow stripes trending SW–NE across BIR. (lower panel) RES transect AA' (see upper panel for location) revealing (1) the shear margin between the BIR and IIS (dashed line); (2) the flat bed beneath BIR; (3) the steep reverse slope of IIS; (4) buckled RES layers beneath flat layers (solid arrow); and (5) a tilting englacial reflection emanating from the bed (dashed arrow).

decrease in age as one moves toward the grounding line (Wearing & Kingslake, 2019). This is consistent with these reflectors being relic basal crevasses, formed in a previous flow configuration, when the grounding line was upstream of its present location. Basal crevasses likely formed as vertical features at former grounding lines and filled with seawater which froze, leading to the high dielectric contrast that generates the reflection in radar data. The ice rise grounding line advanced through this region and, once grounded, basal crevasses were deformed by vertical shear leading to their present day tilt.

Also found within these regions of bright reflectors are troughs in internal layering and layers that intercept the bed. These features are continuous across radar lines. It is thought that these features form as a result of concentrated basal melting at former grounding lines, as observed at former shear margins on the Siple Coast

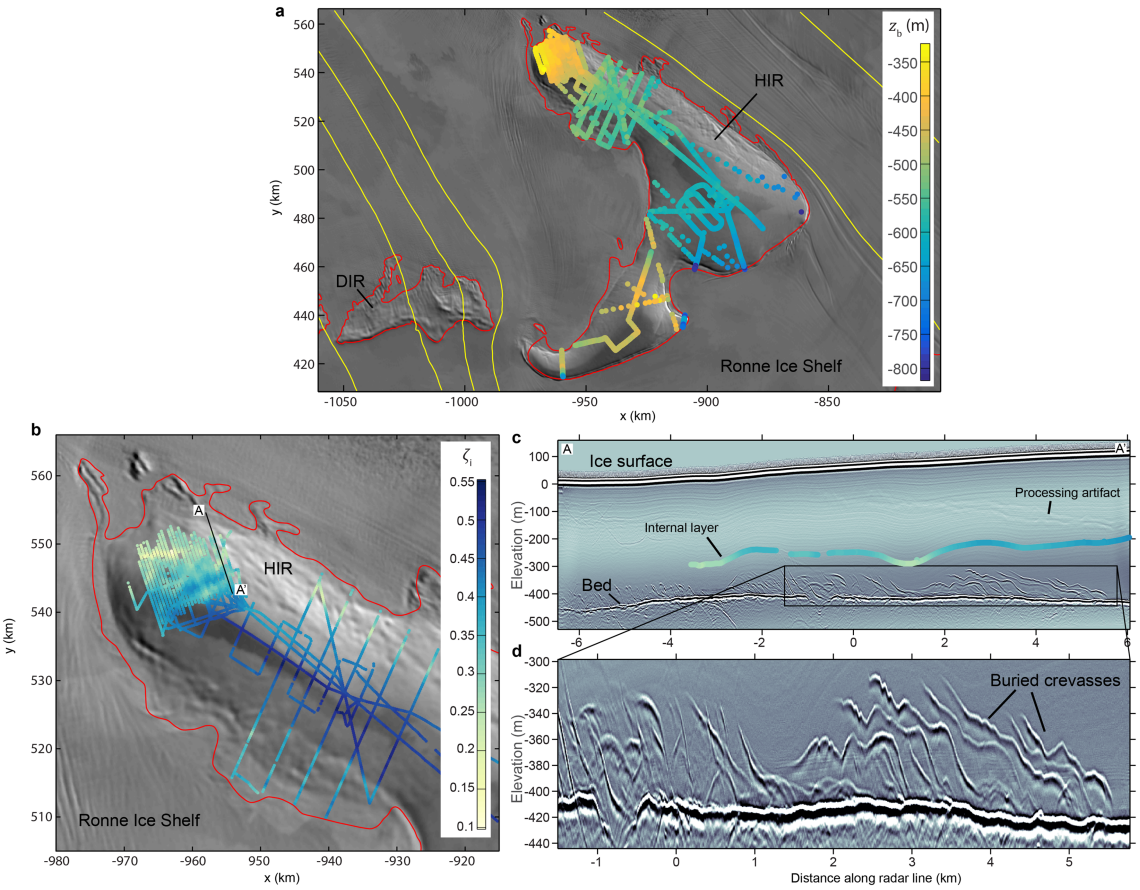

Figure 7. Bed topography and englacial structure of Henry Ice Rise (HIR). (a) Bed topography of HIR from data published as part of the Bedmap2 compilation (Fretwell et al., 2013) and 700 km of ground-based ice-penetrating radar conducted in 2013/2014 and 2014/2015 (Kingslake et al., 2018). Yellow curves are flow lines. Colors show the elevation of the bed above sea level. (b) The normalized elevation of an isochronal internal layer. (c) A radargram showing the internal layer mapped in (b) and relic basal crevasses along the line A-A′ (see (b) for location). (d) A close-up view of the buried relic crevasses. In (a) and (b), the background image is the MODIS Mosaic of Antarctica and the grounding line is shown in red. Adapted from Kingslake et al. (2018).

(Catania et al., 2006). The spatial distribution of relic basal crevasses and melt synclines (Figure 7) suggests ungrounding of the northern basal high, as part of a complete or only partial ungrounding of HIR (Wearing & Kingslake, 2019). We expect ice rises to remain grounded over their high points if they form during a period of ice sheet retreat (Favier & Pattyn, 2015), so these observations suggest complete ungrounding, but we cannot rule out partial ungrounding.

The timing of the grounding line advance surrounding HIR toward its present-day position is estimated to be 6 ± 2kyr (Wearing & Kingslake, 2019); based on a model that simulates the vertical deformation of basal crevasses from their height at formation to the height as observed with RES, while accounting for uncertainty in accumulation, firn density, RES-derived depth, ice-thickening history, initial crevasse height and glacial isostatic adjustment (GIA).

Overall, ground-based RES surveys of HIR and KIR have highlighted stark differences in their internal structure that has been interpreted to be reflective of the two features having contrasting recent flow histories.

5. Cosmogenic Nuclide Evidence of Ice Sheet Reconfiguration

5.1. Cosmogenic Nuclide Methods

In situ cosmogenic nuclide dating of formerly exposed rock and sediment is the only feasible method to date the timing and trajectory of past ice thickness changes in Antarctica. Cosmogenic nuclides are formed in material at the Earth's surface through interaction with secondary cosmic radiation. The flux of cosmic

radiation decreases exponentially in the subsurface as particles interact with the solid Earth. Many cosmogenic nuclides are produced through this interaction, and their concentration in surface rocks can be used as a chronometer indicating the duration of time spent at or within the upper few meters of Earth's surface (Lal, 1991). The method is widely used to reconstruct ice histories because glaciers are highly erosive and generally effective at eroding their beds deeper than a few meters. Therefore, erratics, moraine boulders, or the ice-molded bedrock left behind as the glacier recedes are usually "fresh," with the cosmogenic nuclide inventory having been fully reset. In this way, given knowledge of production rates, the measured concentration of cosmogenic nuclides that have built up subsequently in the dated surface can be used to determine an apparent "exposure age" for that surface. The apparent exposure age may closely date ice retreat or thinning from that position providing the surface has subsequently remained continuously exposed with minimal rock surface erosion. The exposure dating method has been used extensively in Antarctica to constrain past ice sheet elevation change by dating erratics deposited on the flanks of nunataks as the ice sheet thinned. In this way, the nunataks act as dipsticks that record the changing elevation of the ice sheet through time, and the approach has proved highly effective at many locations in Antarctica (Hein, Marrero et al., 2016; Jones et al., 2015; Balco, 2011; Mackintosh et al., 2007; Stone et al., 2003).

Exposure dating in Antarctica is sometimes complicated by ineffective erosion beneath and burial by non-erosive ice. In this case, the cosmogenic nuclide inventory is not fully reset between periods of glacial cover. Where erratics and sediment have been buried by cold-based ice, the assumption of continuous exposure since deposition is violated, and exposure dates from these surfaces will not date the last thinning of the ice sheet. These and other processes can introduce geological scatter into cosmogenic nuclide data sets, which complicates the interpretation of exposure ages in terms of ice sheet thinning. Measurement of multiple cosmogenic nuclides with different half-lives can be used to assess whether a rock surface has experienced a simple exposure history involving continuous surface exposure or a complex exposure history involving periods of burial under ice. In the latter case, the shorter-lived isotope will preferentially decay when buried by ice, causing a detectable change in the isotopic ratio (Lal, 1991). Most studies to date have used the cosmogenic $^{26}Al/^{10}Be$ pairing, since both isotopes are produced in quartz and are easily measured in the same rock. However, the half-life of ^{26}Al (0.705 Ma) is just half that of ^{10}Be (1.389 Ma), so only very long periods of burial on the order of hundreds of thousands of years can be detected using this method. More recently, measurement of in situ ^{14}C in quartz has become possible, and its short half-life (5,730 years) makes it highly sensitive to exposure and burial over the past ~25 ka. For example, ^{14}C paired with a longer-lived isotope, such as ^{10}Be, can detect burial periods as short as a few thousand years, making it highly useful for unravelling ice sheet change over the Late-glacial to Holocene period (Goehring et al., 2011; Goehring et al., 2019; White et al., 2011).

Most cosmogenic nuclide studies to date have focused on measuring ^{10}Be in subglacially derived, sometimes striated cobbles deposited on bedrock on the flanks of Antarctic nunataks. The cobbles are preferred because they often retain a subangular to subrounded shape that is typical of subglacial sediment transported by erosive, warm-based ice. These erosive conditions should produce fresh surfaces with minimal nuclide inheritance. The preservation of striations also indicates minimal erosion of the rock surface after deposition. Exposure dates from locations where these sample characteristics are common can produce clear thinning histories with little geological scatter in exposure age results (e.g., Hein, Marrero, et al., 2016; Jones et al., 2015). In other settings, the success of the method is highly variable. For example, in the Pensacola Mountains, Balco et al. (2016) and Bentley et al. (2017) independently sampled altitude profiles in the Williams Hills that indicated at least 450 m of thinning occurred from the LGM through the Holocene, while a similar altitude profile from the Schmidt Hills, just tens of kilometers downstream, yielded ^{10}Be exposure ages that predate the last glacial cycle, and imply no thinning at all, which is hard to reconcile with the data from Williams Hills. The contrast is likely to do with specific flowlines of ice streams and tributary glaciers, as well as transitions between warm- and cold-based ice (Bentley et al., 2017). It is situations like these where the measurement of in situ ^{14}C can be advantageous (e.g., Balco et al., 2016). Recent analysis of in situ ^{14}C from the Schmidt Hills indicates at least 800 m of thinning occurred after the LGM [Nichols et al., 2019]. Likewise, in situ ^{14}C analysis of rocks from the Shackleton Range indicate the Slessor Glacier thinned by at least 300 m, and perhaps as much as 650 m, following the LGM; this result contrasts with long-lived isotopes that imply no thinning at all and demonstrates the utility of in situ ^{14}C at sites where nuclide inheritance is problematic (Hein et al., 2011, 2014; Nichols et al., 2019).

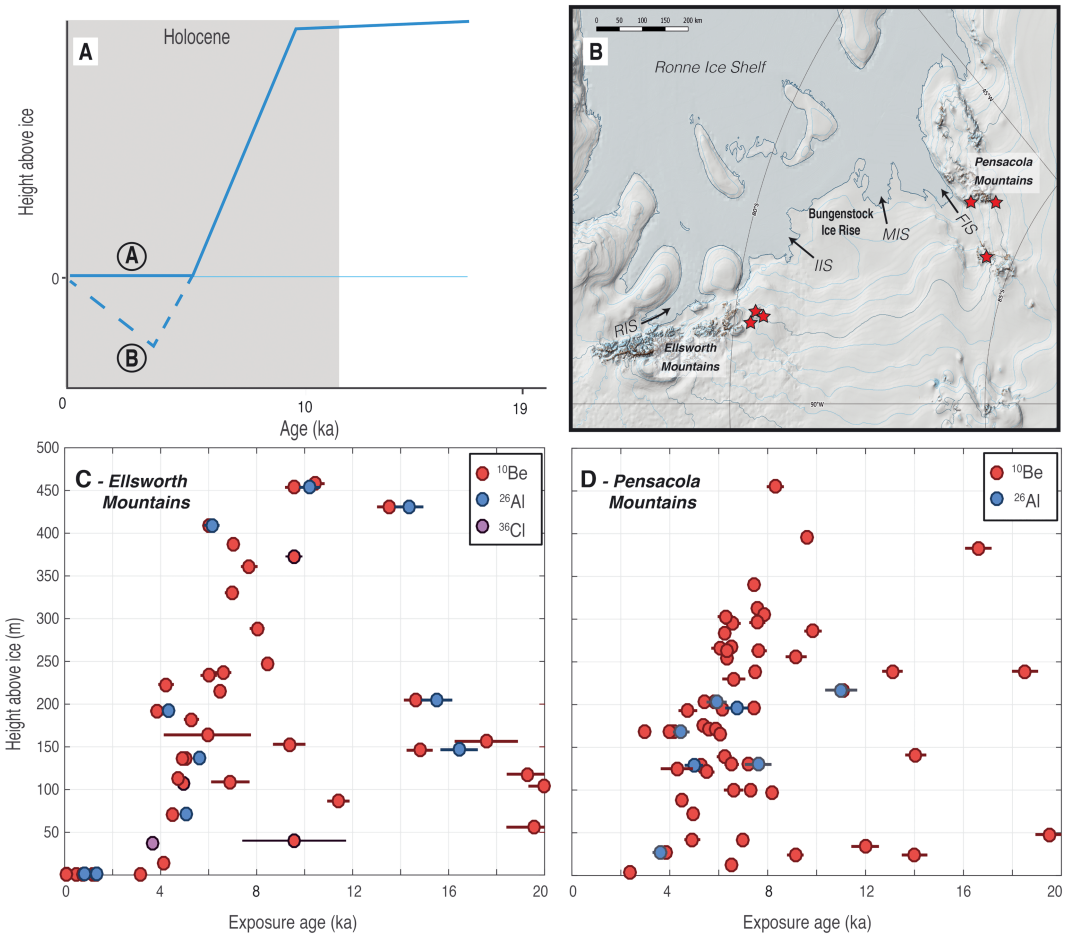

Figure 8. Cosmogenic nuclide measurements of Holocene ice sheet behavior. (a) Hypothetical age-elevation plot with two groups of scenarios. In both cases, the ice sheet thins from a former (LGM) thicker configuration to reach the present ice sheet elevation in the Late Holocene. In scenario "A," the ice sheet then stays at the present-day level for a few ka to the present day. In scenario "B," the ice sheet thins to below present elevations in the Late Holocene and rethickens to the present-day. (b) Location map of the Holocene age-elevation cosmogenic profiles in the southern WS. (c) Age-elevation plot from the southern Ellsworth Mountains. Data compiled from Bentley et al. (2010); Hein, Woodward, et al. (2016); and Hein, Marrero, et al. (2016). (d) Age elevation plot from the Pensacola Mountains. Data compiled from Balco et al. (2016) and Bentley et al. (2017). Two samples emerging from actively ice-cored moraines have been excluded from the plot because they may record buried ice ablation rather than ice sheet thinning.

5.2. Data From the SWSE Sector and Surroundings

Changes in the Holocene elevation of the ice sheet surface in the heart of the SWSE have been studied in the southernmost Ellsworth Mountains, notably the Patriot Hills, Marble Hills and Independence Hills (Bentley et al., 2010; Hein, Woodward et al., 2016; Hein, Marrero, et al., 2016; Johnson et al., 2019). Analysis has also been carried out on material from the Pensacola Mountains, to reveal the thinning history at Mount Bragg and Mount Harper, recording past elevation change of the Academy Glacier, and the Williams Hills and Thomas Hills adjacent to the FIS (Balco et al., 2016; Bentley et al., 2017). In all areas, the pattern is similar but with minor differences in timing, namely that the altitude profiles show ice sheet thinning that reached the level of the present-day ice in the Late Holocene (Figure 8). The data are consistent with the two Holocene ice history scenarios noted previously but currently cannot distinguish between them. The first scenario is that the ice reached present-day ice level in the Late Holocene and thinned no further, staying at the same level since that time to present (scenario A in Figure 8a). A second scenario is where the ice thinned below the present-day level in the Late Holocene and only subsequently thickened to present levels (scenario B in Figure 8a).

In the Ellsworth Mountains, the more recent work relies on cosmogenic nuclide $^{26}Al/^{10}Be$ pairing on quartz and ^{36}Cl from limestone samples of unweathered and often striated glacial erratics (Hein, Marrero et al.,

2016). Field observations and airborne RES show that these erratics have been derived from the glacier base and been brought to the ice surface in a blue-iced ablation area. On the mountain slopes above the present ice surface such erratics have been deposited as a veneer of perched blocks. The upper limit of such fresh erratics demonstrates the maximum thickness of the Weddell Sea sector of the ice sheet during the LGM; a state that persisted until the beginning of the Holocene. Cosmogenic exposure-age transects from the upper limit to the present ice record the history of thinning of the ice during the Holocene at a location close to the present grounding line in Hercules Inlet.

The upper limit of unweathered erratics shows that the ice was up to ~475 m thicker than present in the southernmost Ellsworth Mountains during the LGM (Bentley et al., 2010; Hein, Marrero, et al., 2016). The range of dates at the upper limit of 49–10 ka encompasses the peak of the LGM at ~21 ka and could imply that thick ice persisted throughout the warming of the late-glacial (~18–10 ka). It seems reasonable to argue that this persistence reflects the increased snowfall and ice accumulation associated with warming as shown in the WAIS ice core (WAIS Drilling Project, 2013). Importantly, the direction of flow of the thicker ice sheet was eastward toward BIR (cf. Siegert et al., 2013). This is shown by erosional landforms, erratic trains of known lithology and the orientation of a blue-iced moraine immediately north of Independence Hills.

The vertical transects, taken together, show that the ice sheet surface in the Ellsworth Mountains began to fall about 10 ka ago and had reached the present level by 3.5 ka. Moreover, there was a pulse of rapid thinning of ~400 m at 6.5–3.5 ka that if extrapolated around the Weddell Sea Embayment, would have contributed 1.4–2 m to global sea level rise (Hein, Marrero, et al., 2016). Interestingly, the geomorphology, changes in direction of ice flow of glaciers into Horseshoe Valley, and the disruption of blue-ice moraines, all linked to the eastward flow of thicker ice, accompanied or followed this sharp pulse of thinning. The most likely reason is that the migration of the grounding line into the troughs of IIS and Hercules Inlet captured the eastward ice flow toward BIR from the Horseshoe Valley.

In the Pensacola Mountains, the ice sheet history is consistent with that inferred for the southern Ellsworth Mountains. The Academy Glacier thinned similarly rapidly through the Holocene and reached present levels by 2.5 ka, while a few 10s of kilometers away, the FIS had thinned at least a few 100 m to within 40 m of present levels in the Williams Hills by 5.2 ka (Bentley et al., 2017; Balco et al., 2016; Nichols et al., 2019). A mid-Holocene pulse of thinning of similar scale and magnitude has also been reported from the Lassiter Coast in the western WSE based on in situ ^{14}C ages (Johnson et al., 2019). Here the ice elevation fell from 385 to 138 m above modern ice between 6.0 $\pm$ 0.5 and 7.5 $\pm$ 0.7 ka before present.

6. Solid Earth Measurements and Modelling

6.1. Ice Dynamics, Solid Earth Deformation, and Sea Level Change

The evidence reviewed above does not allow us to distinguish between the two scenarios proposed for the recent glacial history of the SWSE. Therefore, in an attempt to fill some of the spatial and temporal gaps in the data, we turn to the insight that can be provided by ice sheet and solid-Earth modelling. Numerical ice sheet models, driven by changes in climate, can be used to predict changes in ice flow and thickness which can be compared with evidence from RES and cosmogenic exposure dating. The solid Earth and sea level response to these changes in ice loading can be predicted using a GIA model and compared with GPS-derived estimates of present-day surface deformation and geological evidence for relative sea level change.

Feedbacks between the ice sheet, the solid Earth and sea level change likely played an important part in controlling the behavior of the SWSE during the late Holocene. Such feedbacks have the potential to stabilize (Gomez et al., 2010) or destabilize (Siegert, 2001) the ice sheet, and both types of behavior have been reproduced by numerical models. Studying the strength of the various feedbacks, via modelling and model-data comparisons, helps us to determine which processes governed the evolution of the WS sector during the late Holocene.

Marine ice sheet instability describes the process whereby grounding line retreat on a reverse bed slope leads to an increase in ice thickness at the grounding line (where the bed deepens upstream) and, hence, an increase in ice flux across the grounding line (e.g., Joughin et al., 2014). If this increase in flux is not balanced by an increase in accumulation, this can lead to runaway retreat until the bed begins to

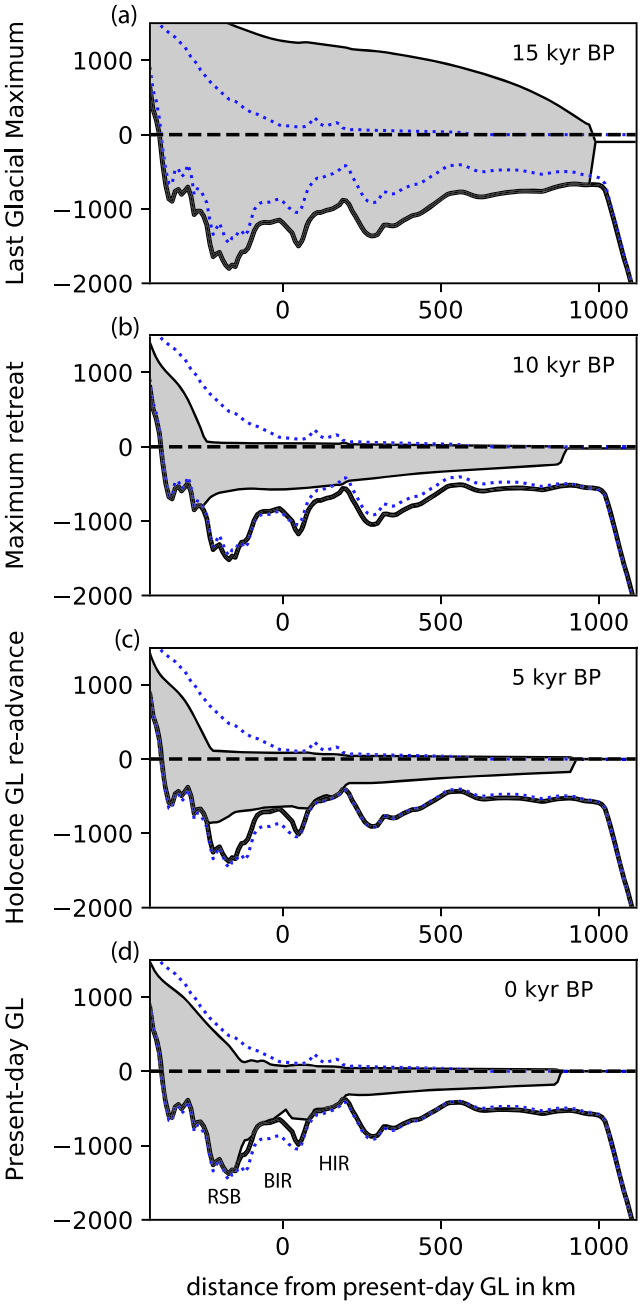

Figure 9. Cross sections of model-predicted ice thickness and bed deformation along a transect that crosses the Robin Subglacial Basin (RSB), Bungenstock Ice Rise (BIR), and Henry Ice Rise (HIR) at 5-kyr intervals during the last deglaciation. Model details are described in Kingslake et al. (2018). The horizontal axis shows distance from the present-day grounding line (GL), units on the vertical axis are meters. The blue dotted line outlines the observed present-day configuration of the ice sheet and seafloor. (a) Last Glacial Maximum configuration, ice sheet grounded near continental shelf edge, seafloor isostatically depressed by several hundred meters. (b) Grounding line located upstream of the RSB, ice shelf persists across the Weddell Sea, seafloor rebounding. (c) Rebound triggers ice shelf regrounding and formation of the HIR. (d) Ongoing rebound and buttressing associated with the formation of the HIR results in formation of the BIR and grounding line readvance to present-day configuration. Adapted from Kingslake et al. (2018).

shallow, and ice thickness reduces, again upstream. Along many of the ice streams in the SWSE the bed deepens inland, so if the marine ice sheet instability was the dominant process controlling ice sheet dynamics, we might expect the grounding line to have retreated continuously from an LGM position somewhere on the continental shelf to a stable position upstream of the present grounding line. Instead, the present-day grounding line is perched part-way along the reverse bed slope that extends from the continental shelf to regions such as the Robin Subglacial Basin (Ross et al., 2012). The reason for the apparently unstable position of the present-day grounding line is likely the presence of the RFIS, which exerts a significant buttressing effect on the grounded portion of the ice sheet, and the presence of large ice rises (Matsuoka et al., 2015). Indeed, Whitehouse et al. (2017) used a numerical flowline model to demonstrate that ice shelf collapse would lead to grounding line retreat behind present but that ice shelf regrowth would rapidly allow the grounding line to readvance to its observed position along the FIS. Kingslake et al. (2018) modeled similar behaviour in the central SWSE (Figure 9).

In addition to the buttressing provided by the RFIS and its ice rises, isostatic uplift in response to ice loss may also have helped to stabilize the WS sector of the ice sheet during the late Holocene. As an ice sheet thins or retreats, the net reduction in surface loading, after accounting for the flux of ocean water into the space left by a retreating ice sheet, triggers viscoelastic rebound. The wavelength of the rebound will depend on the thickness of the lithosphere, while the magnitude and time dependence will be controlled by the viscosity structure of the mantle (Nield et al., 2018). In tandem with the uplift of the bed, the decreasing mass of the ice sheet leads to a decrease in the gravitational attraction exerted by the ice sheet on the ocean, and hence a drop in the local height of the geoid, that is, the sea surface (Gomez et al., 2010). The net effect of these two GIA-related processes is a decrease in the water depth at the grounding line, which, if large enough, has been hypothesized to have the potential to slow, or even reverse, unstable grounding line retreat (Gomez et al., 2015; Kingslake et al., 2018; Konrad et al., 2015). In addition to reducing water depth at the grounding line, the reduction in water depth offshore can help to promote ice rise formation, thus increasing the buttressing effect of the ice shelf (Favier & Pattyn, 2015).

The spatiotemporal history of isostatic rebound during the late Holocene and the degree to which it has played a role in governing the evolution of the SWSE is poorly known. The spatial pattern of rebound will depend on the history of both ice thickness change and grounding line retreat across the Weddell Sea embayment, a region that is currently covered by the RFIS. Ice sheet modelling provides some insight into possible configurations of past retreat (e.g., Golledge et al., 2014; Maris et al., 2014; Pollard et al., 2017), with large-scale constraints on past ice thickness and grounding line extent available from ice cores recovered from ice rises (e.g., Mulvaney et al., 2002).

The second factor that controls the rate of isostatic rebound is the rheology of the solid Earth. Mantle viscosity is hypothesized to be relatively high across the southern part of the SWSE (~10^{21} Pa s; Whitehouse et al., 2019), but there is limited information on the rheology beneath the outer part of the embayment due to poor coverage by seismic stations (Shen et al., 2018). High mantle viscosity can be related to a long decay time

(McConnell, 1965) and, hence, rebound in response to post-LGM ice loss is likely to be ongoing today across the southern portion of the SWSE, with the caveat that the timing of post-LGM ice loss is poorly known. When seeking to reconstruct past ice sheet change using contemporary rates of solid Earth deformation, the trade-off with Earth rheology leads to significant non-uniqueness (Whitehouse, 2018), with an additional complication being that the loss of ice close to flotation will trigger a limited isostatic response. Feedbacks between ice dynamics and isostatic rebound will be greatest in regions where there has been a significant decrease in the thickness of ice above flotation.

In summary, isostatic rebound may have reduced the rate of grounding line retreat, promoted the likelihood of ice rise formation, or even triggered grounding line readvance across the SWSE and wider WS sector during the late Holocene. If readvance did take place and was accompanied by sufficient ice thickening above flotation, this will have damped the rebound process, and contemporary uplift rates would be smaller than expected in a scenario of monotonic ice loss and retreat. The following two sections briefly outline what is known about isostatic rebound across the WS sector, and how these observations compare with recent modelling efforts.

6.2. Data From the SWSE and Surrounding

Records of isostatic rebound across the SWSE are limited to a small number of GPS sites that record contemporary solid Earth deformation. The traditional approach of reconstructing millennial-scale solid Earth deformation via the interpretation of relative sea level records is not possible due to the complete lack of exposed coastline in the region. In other regions, relative sea level records have traditionally been used to determine the relaxation time and, hence, the viscosity of the mantle (e.g., Mitrovica & Forte, 2004). The short time span of the GPS data in the SWSE provides no insight into the relaxation time of the mantle, and this exacerbates the issue of non-uniqueness when seeking to use the GPS rates to infer the history of past ice sheet change.

The sparse spatial coverage of bedrock GPS sites is related to the lack of outcrops in the region; currently, no techniques exist for measuring isostatic rebound beneath regions of grounded or floating ice. It is logistically challenging to regularly access the bedrock GPS sites to download data and service the instruments. This is changing as the majority of instruments now have the capacity to transmit data and state-of-health information in real time, but there are significant historical data gaps in many records, and these are reflected in the large uncertainties associated with deformation rates at many sites. Published GPS rates across the region span −2.20 to +7.04 mm/year but typically have uncertainties on the order of 1–2.5 mm/year (Bradley et al., 2015; Wolstencroft et al., 2015). Extending the temporal and spatial coverage of measurements that reflect the contemporary pattern of solid Earth deformation across the WS sector would provide invaluable insight into recent ice sheet change and the stability of the current ice sheet configuration. Spatially continuous estimates of isostatic rebound are beginning to be derived via data inversion, whereby satellite gravimetry and altimetry data are combined to simultaneously invert for contemporary ice mass loss and the GIA signal, often also incorporating GPS observations (Engels et al., 2018; Gunter et al., 2014; Martín-Español et al., 2016; Sasgen et al., 2017). Uncertainties are large, due to assumptions related to the interpretation of satellite data, but at least they can be formally quantified in this independent, data-driven approach.

6.3. Modelling and Plausible Ice Sheet Reconstructions

GIA modelling can be used to predict the pattern and magnitude of isostatic deformation across the WS sector for the post-LGM period. A "forward" GIA model requires inputs of ice history and Earth rheology, and this permits the calculation of spatially varying sea level change and solid Earth deformation (e.g., Argus et al., 2014; Briggs et al., 2014; Ivins et al., 2013; Whitehouse, Bentley, Milne et al., 2012). To better understand the impact of isostatic rebound on ice dynamics, GIA model output relating to the uplift history of the WS sector could be prescribed as an a priori boundary condition for ice sheet modelling. However, there is currently considerable uncertainty regarding the pattern of GIA-related solid Earth deformation across the wider WS sector.

GIA model predictions of present-day uplift rates across the WS sector vary significantly in both spatial pattern and magnitude (Whitehouse et al., 2019). The majority of models predict maximum present-day uplift rates in the region of the HIR, KIR, and BIR, with predicted rates peaking at >10 mm/year (Argus et al., 2014; Whitehouse, Bentley, Milne, et al., 2012). Models that incorporate 3-D variations in mantle rheology may predict both faster (Geruo et al., 2013) and slower (van der Wal et al., 2015) uplift rates compared

with calculations that combine the same ice history with a simple 1-D profile of mantle viscosity. The predictions of Ivins et al. (2013) have a very different spatial pattern, with maximum uplift rates of only ~5 mm/year predicted for the southwest Weddell Sea region and negligible (<2 mm/year) rates predicted for the central SWSE. The history of post-LGM deformation will also vary considerably between models. These differences between GIA model predictions arise primarily due to a lack of constraints on post-LGM ice sheet configuration, which has led to there being significant differences between the ice history models adopted in the different GIA models. None of the models provide a good fit to the regional uplift pattern documented by GPS (Martín-Español et al., 2016).

Most Antarctic GIA modelling studies are motivated by the desire to test a new data-constrained or modelling constrained reconstruction of past ice sheet change within a GIA framework (e.g., Whitehouse, Bentley, & Le Brocq, 2012; Whitehouse, Bentley, Milne, et al., 2012). In contrast, Bradley et al. (2015) sought to explain the surprising observation that a GPS site in the Ellsworth Mountains, a region expected to be uplifting in response to post-LGM ice mass loss, was subsiding. They calculated the isostatic response to a suite of hypothesized ice history scenarios, including an approximation of the two scenarios proposed by Siegert et al. (2013) and found that the GPS observations could not be explained by monotonic post-LGM ice loss, that is, scenario A. Instead, the data required there to have been a period of either ice thickening or re-advance during the late Holocene (Bradley et al., 2015). The study was unable to provide detailed insight into the position of the grounding line during the late Holocene, primarily due to the fact that any advance or retreat of grounded ice close to flotation would have left a negligible isostatic fingerprint.

There is clearly a significant range in model predictions of isostatic rebound across the WS sector leading to uncertainty in efforts to quantify the impact of this rebound on ice sheet dynamics during the late Holocene. Many ice sheet models include an isostatic component (e.g., Bueler et al., 2007), but they are unable to account for the second feedback associated with GIA, which is the local drop in the height of the sea surface associated with a decrease in the mass of the ice sheet. This can only be determined by running a GIA model that accounts for the global redistribution of meltwater across the ocean. The most self-consistent approach to determining feedbacks between GIA and ice dynamics is therefore to run a coupled model (e.g., de Boer et al., 2017; Gomez et al., 2013). However, a significant limitation of this approach, aside from the uncertainty associated with climate forcing, is the need to know the correct Earth rheology. Upper mantle viscosity across Antarctica is thought to vary by >3 orders of magnitude (Hay et al., 2017; van der Wal et al., 2015; Whitehouse et al., 2019). The associated range in mantle relaxation times significantly perturbs the strength of the feedback between isostatic deformation and ice dynamics in different regions of Antarctica (Gomez et al., 2015; Konrad et al., 2015; Pollard et al., 2017) and motivates the need for a coupled ice sheet-GIA model that incorporates 3-D Earth structure. Gomez et al. (2018) use such a model to quantify the effect of incorporating 3-D variations in mantle viscosity compared with a more common 1-D radial profile of mantle viscosity. Differences in predicted ice thickness in the southern Weddell Sea region are on the order of several hundred meters during the Holocene, with implications for grounding line position. Similarly, they predict differences in relative sea level and contemporary uplift rates between the 1-D and 3-D models on the order of tens of meters during deglaciation, and several millimeters per year at the present day, respectively. Such models are rapidly enhancing our ability to explore the drivers of ice sheet change in the WS sector, but a crucial outstanding issue is the need to simultaneously represent feedbacks between ocean forcing and ice shelf evolution (Asay-Davis et al., 2016). The buttressing provided by ice shelves plays a significant role in controlling the stability of the ice sheet (Wright et al., 2014), and ice shelf thickness directly determines whether ice rises are able to form as a result of isostatic rebound.

We close this section by reviewing the results of ice sheet modelling studies that are not coupled to a GIA model but that do incorporate some component of solid Earth rebound. It is interesting to note that model-derived ice sheet reconstructions predict grounding line retreat behind present, and subsequent readvance, at some point during the Holocene, at a range of locations around the southern Weddell Sea (Golledge et al., 2014; Kingslake et al., 2018; Maris et al., 2014; Pollard et al., 2017). These studies use different numerical ice sheet models, and they differ in their approach to climate forcing, ice sheet basal conditions, and ice shelf dynamics, but all represent an attempt to reconstruct the history of the WAIS since the LGM. This is not to say that all modelling attempts reproduce grounding line retreat behind present; the ensemble analysis of Briggs et al. (2014) does not appear to predict Late Holocene readvance in the wider WS sector, while in the studies of Pollard et al. (2017) and Kingslake et al. (2018) model scenarios that involve faster rates of rebound

predict slower rates of ice loss and no retreat behind present. This is due to the damping effect of the rapid rebound.

In this section, we have summarized the ice sheet and solid Earth modelling efforts that provide insight into the processes controlling recent ice sheet change in the SWSE and wider WS sector. As may be expected, standalone and coupled ice sheet models are able to reproduce a range of scenarios that encompass the retreat histories suggested by the glaciological and geological data documented above. However, it appears that the rate of isostatic rebound potentially plays a crucial role in determining the details of the retreat. On one hand, isostatic rebound can act to slow the rate of grounding line retreat, which would be compatible with the hypothesis that the grounding line is currently in its most retreated position since the LGM (scenario A). Alternatively, isostatic rebound may have helped trigger ice rise formation and grounding line readvance subsequent to retreat behind present at some point earlier in the Holocene (scenario B). Ultimately, additional data are needed to resolve the details of recent ice sheet change and provide further insight into the strength of the feedbacks operating between the ice sheet, the solid Earth, and the ocean.

7. Holocene Glacial History

7.1. Ice Flow at and Before Mid-Holocene

Geophysical data from the ice sheet and exposed rocks point consistently to major ice sheet change in the WS sector at around 5,000 years. Buckled layering in the BIR, beneath continuous layers dated to around 4,000 years, coupled with palaeoflow stripes across the ice rise, are clear indicators that the ice location was once covered by fast flowing ice. The flow stripes point to an origin from the IIS tributaries, parallel to the modern flow of MIS. This is also consistent with basal features that can tentatively be correlated between BIR and Horseshoe Valley. We are unable to explain whether the ice across BIR was floating (i.e., a fast-flowing section of an ice shelf emanating from upstream IIS) or an ice stream grounded across the Robin Subglacial Basin and BIR, however.

Beneath the ice divide on KIR a prominent Raymond Arch suggests stable flow here during at least the past 2–3 kyr (Kingslake et al., 2016). Further north along the KIR divide, polarmetric phase-sensitive radar and active seismic surveys reveal a transition in englacial fabric at around 200- to 230-m depth (Brisbourne et al., 2019). These authors interpret the fabric beneath this depth as evidence of a change in past flow conditions. Specifically, the observations can be explained by previous flow aligned approximately along the ice divide, away from IIS. Tracing stratigraphy back to the divide used to date the formation of Raymond arches (Kingslake et al., 2016) indicates that the change from this previous SW–NE flow regime occurred around the time of Raymond Arch formation (2–3 kyr). There is no englacial stratigraphic evidence for past fast flow at KIR and because 2–3 kyr is not long enough for such evidence to flow out of KIR, we can conclude that at least immediately prior to the onset of ice divide flow (and the formation of the Raymond arches), flow was not fast over KIR. This does not rule out a previous period of fast flow over KIR and even regrounding of the ice shelf in this location if it occurred long enough in the past for any englacial evidence of fast flow, as is seen in BIR and HIR, to advect out of the region surveyed by Kingslake et al. (2016).

The lack of mature Raymond Arches on HIR suggest that ice flow has not been stable here for at least the characteristic time of the ice rise (Martín et al., 2009), approximately 4.5 kyr. The complex englacial structure of HIR can be explained if the grounded area of the ice rise was smaller in the past and readvanced toward its current position at around 6 kyr. Without a previously smaller ice rise and a subsequent advance of the grounding line to its present location, it is difficult to explain the spatial pattern of the interception between isochrones and steeply dipping englacial layers interpreted as marine ice-filled relic basal fractures (Wearing & Kingslake, 2019).

Two interpretations are possible as to the minimum extent of HIR during the Holocene. In one interpretation the ice rise ungrounded completely; this can explain all the unusual englacial structures observed. Alternatively, the ice rise ungrounded from the northern subglacial topographic high but remained grounded over deeper regions. Based on our limited understanding of ice rise formation and subsequent evolution, this appears unlikely; it is inconsistent with recent idealized modelling of ice-rise dynamics (Favier & Pattyn, 2015). While a smaller than present HIR that nonetheless persisted throughout the Holocene cannot be ruled out, until a deeper understanding of ice-rise flow dynamics and independent constraints on the past spatial extent of the ice rise are obtained, the interpretation that the ice rise ungrounded completely during

initial post-LGM ice sheet retreat and later regrounded, perhaps due to GIA(section 6), is consistent with this argument.

Some modelling studies pertain to the question of whether ice rises in the Weddell Sea ungrounded during the Holocene (section 6.3). For example, Kingslake et al. (2018) examined the hypothesis of a complete Holocene ungrounding of HIR and its implications using an ice sheet model that incorporates simplified GIA physics. They were able to reproduce the situation where BIR, KIR and HIR ungrounded after the LGM. Despite limitations related to resolution and bed topography, this suggests ungrounding was possible, but depends sensitively on, among other factors, the solid Earth and ice properties prescribed in the model, the climate, and the LGM extent of the ice sheet.

7.2. Ice relaxation Model: Mid-Holocene to Today

In this model, gradual retreat of the grounding line to its position 5,000 years ago, with associated ice thickness reduction and crustal uplift, led to relatively thin ice in the locations of the ice rises. This caused rerouting of water from the palaeo IIS trunk into the Robin Subglacial Basin, and both slow cold-based flow over the BIR and the creation of today's fast flowing IIS along the subglacial basin. Evidence in support of this idea comes from the shear margin between IIS and BIR, which is a hydrological one, and from the Siple Coast, where subglacial water migration is thought to be key in the shutting down and activation of ice streams (Anandakrishnan & Alley, 1997). It is possible that either Scenario MAX or Scenario MIN of Hillenbrand et al. (2014) at 5,000 years is consistent with this model (Figure 3).

7.3. Ice sheet Retreat and Readvance Model: Mid-Holocene to Today

An alternative explanation is that the ice margin retreated upstream of today's position, deglaciating the Robin Subglacial Basin. During this time, an ice shelf persisted across the current location of the BIR/KIR/HIR, and it became grounded sometime during the middle-to-late Holocene due to post-LGM isostatic uplift. This grounding led to the buildup of the ice rises, blocking fast-flowing ice, and leading to the rerouting of the IIS to the west of BIR, and MIS to its east. Evidence in support of this includes the englacial stratigraphy discovered within HIR and the buckled internal layers at the northern edge of BIR. In addition, the low GPS uplift rates recorded in the Ellsworth Mountains have been interpreted to reflect the damping effect of ice sheet readvance on post-LGM rebound (Bradley et al., 2015). Models that incorporate both ice sheet dynamics and glacial rebound reveal how this scenario is possible (e.g., Kingslake et al., 2018), but the details depend on poorly quantified factors such as Earth rheology, seafloor topography, and ocean-ice shelf interactions.

7.4. Cosmogenic Nuclide Evidence: Mid-Holocene to Today

Cosmogenic nuclide evidence indicates that the current ice surface is close to that first achieved at 3.5 (Ellsworths) or 2.5 ka (Pensacola; Figure 8). The data also point to major ice flow direction change consistent with former flow across what is now the BIR. However, the data do not favor one or other hypothesis (relaxation vs. readvance) concerning the history of ice changes in the last few thousand years. There is nothing from the geomorphology or from cosmogenic nuclide dating to rule out thinning to below the 3.5 ka (2.5 ka) level. On the other hand, the geomorphological evidence of blue-iced moraine stability (Hein, Woodward, et al., 2016) and the early Holocene age of some blue ice itself (Winter et al., 2016.) rules out extensive deglaciation with open fjords.

8. Hypotheses Synthesis

On the face of it, the two scenarios for Late Holocene change in ice sheet flow seem irreconcilable. One involves a gradual relaxation of the ice sheet, with ice dynamics and flow modified by the rerouting of basal water. The other relates to deglaciation upstream of the modern grounding line, followed by regrounding through postglacial uplift of relatively high ground to form ice rises. However, there is a consistent message, from multiple RES data sets and cosmogenic analyses, for major ice-flow dynamic change and ice sheet reconfiguration within the SWSE, and the wider WS sector of the WAIS, around the mid-Holocene. Buckled RES layers within ice rises point to former enhanced flow where the ice now flows slowly; palaeo-flow stripes on the BIR indicate the former direction of that enhanced flow, and cosmogenic data reveal how upstream ice sheet flow has changed direction from flowing east toward the BIR, to flowing west into the modern IIS. RES also reveals Raymond bumps within the KIR, HIR and BIR that are relatively recently formed, suggesting ice rise formation in the last few thousand years.

The major difference between the two scenarios is that, in one, the ice sheet grounding line progressively retreated from its LGM position to its present grounding line, whereas in the other the grounding line retreated upstream of present limits and subsequently readvanced to the present. While numerical modelling demonstrates how this latter scenario is possible, there are no conclusive data for either.

While this disagreement might seem challenging to reconcile, the two scenarios have one important point of agreement beyond an acknowledgement of mid-Holocene ice sheet change; that is, they can both accommodate a level of post-LGM isostatic uplift. In the former scenario, such uplift could lead to topographic influences on basal water flow and ice sheet dynamics; in the latter it would lead to regrounding of an ice shelf and backfilling of grounded ice upstream. This agreement stems from the fact that the WS sector is a particularly sensitive part of the ice sheet to relative sea level (Wright et al., 2014). Indeed, the grounding line is known to oscillate by several kilometers each day as a consequence of tides lifting up otherwise grounded ice during high tide and dropping it to the bed on low tide. This process has been observed over the BIR (Brunt et al., 2011) and the FIS (Jeofry, Ross, Le Brocq, et al., 2018).

Given that the Robin Subglacial Basin is occupied by grounded ice that is relatively close to flotation (Ross et al., 2012), if it were to deglaciate (i.e., the ice sheet was to lift off the bed), it is unlikely there would be any major isostatic signal. Hence, there may simply be no conclusive isostatic record in favor of one scenario.

It is also unlikely that RES or more cosmogenic data from exposed surfaces will provide a resolution to the problem. However, if we could obtain samples from key regions of the subglacial environment, and date them, we may be able to provide a solution. Conceptually, the best way to use cosmogenic nuclides to distinguish between the different scenarios is to drill the margins of some of the glaciers or ice streams where we have ice sheet thinning histories. Retrieval of bedrock from below the margins will allow a test of the hypothesis that the ice has been thinner than present in the Holocene; any bedrock exposed in the Holocene and then recovered by ice will still contain a significant inventory of in situ ^{14}C isotopes. If the bedrock had been exposed in a previous thinning/interglacial, then the ^{14}C would have decayed (as its half-life = 5730 years). Drilling at various depths to find the boundary between ^{14}C-containing bedrock and that at lower elevation with no ^{14}C would enable determination of the minimum thickness reached. In addition, if subglacial access to the Robin Subglacial Basin or beneath the BIR, KIR or HIR is possible, where soft marine sediments deposited when the ice sheet was not present are thought to exist (Siegert et al., 2016), it may be possible to date the material by radiocarbon methods—certainly obtaining a Holocene date from such a sample would be a significant piece of information in support of the readvance hypothesis. Sampling the ice from a borehole drilled to access the bed (either as a full core or as chippings from a rapid drilling system) may permit isotopic analysis to reveal signals associated with either scenario; for example, if HIR was completely ungrounded during the Holocene, its deep ice would have been deposited on the surface while on the main ice sheet at higher elevations than is plausible in an ice rise. This would leave an isotopic signature. Finally, sampling ice from the hypothesized relic basal crevasses and measuring borehole temperatures on HIR and BIR may be key to determining the grounding history of these crucial areas.

9. Summary

The WS sector of the WAIS is known to be one of the most sensitive regions of the ice sheet to ocean-driven melting and grounding line recession, with the SWSE being particularly vulnerable. However, despite the SWSE being at a threshold of change, owing to the present grounding line of IIS being perched at the top of a major steep reverse bed slope, satellite altimetry shows that the region is, at present, not experiencing significant change like in the Amundsen Bay region of WAIS. However, satellite imagery of surface flow stripes, coupled with RES evidence of buckled internal layers and corroborated by cosmogenic dating of exposed surfaces, point to recent (mid-Holocene) and substantial ice-dynamic change in the SWSE.

Two scenarios to explain this change have emerged. First, the ice sheet gradually relaxed from its LGM position involving fast-flowing ice across the BIR. Because of ice sheet thinning, water and ice flow were routed around what is now BIR to set up the ice sheet as we now see it. Alternatively, ice retreated inland of the present margin, forming an ice shelf over the Robin Subglacial Basin and the BIR/KIR/HIR, whereupon isostatic uplift led to regrounding over the ice rises and the present flow regime.

While available glaciological and geophysical information cannot distinguish between these scenarios, they do have some areas of commonality. First, all evidence points to mid-Holocene change to the flow and form of the SWSE. Second, both scenarios can accommodate postglacial uplift to drive either ice dynamic alteration on one hand, or grounding on the other. Third, it is also possible that both scenarios may have acted together, with uplift leading to regrounding and ice direction change. Such a situation may account for buried crevasses within HIR, thought to be formed within an ice shelf and captured as a consequence of grounding, as well as the shear margin between IIS and BIR, which appears to be controlled solely by ice sheet thermodynamics and the supply of water, rather than topography. Fourth, we should appreciate that the SWSE experiences significant (>10 km) grounding line change as a consequence of tides, and much of the region is relatively close to the level of flotation now; hence, migration of the grounding line upstream of modern limits could easily occur without much isostatic signal today.

It is curious that the SWSE currently appears to show no sign of significant mass loss. The recent readvance hypothesis may be consistent with this, as the ice sheet would have effectively experienced expansion to its present limits. As ice sheet modelling has shown, however, this is unlikely to make the sector more stable to the influx of warm ocean water; if this happened, we still expect, under either scenario, the SWSE to experience grounding line retreat across the Robin Subglacial Basin.

Glossary

LGM	Last Glacial Maximum, around 20,000 years ago
Holocene	The Last ~10,000 years of Earth history
BIR, HIR, KIR	Bungenstock, Henry, and Korff ice rises
WS	Weddell Sea
WAIS	West Antarctic Ice Sheet
EAIS	East Antarctic Ice Sheet
SWSE	Southern Weddell Sea Embayment
RIS, IIS, MIS, FIS	Rutford, Institute, Möller, and Foundation ice streams
RES	Radio-echo Sounding
GIA	Glacial Isostatic Adjustment
Al, Be, C	Aluminium, Beryllium, Carbon
GPS	Global Positioning System
ka	thousand years ago
Ma	million years ago
Scenario MAX	Maximum LGM extent of ice
Scenario MIN	Minimum LGM extent of ice
Scenario A	Gradual retreat of ice in the Holocene from LGM values
Scenario B	Holocene retreat upstream of today's grounded limit with subsequent ice expansion
MISI	Marine Ice Sheet Instability—associated with ice retreat across retrograde bed slope below sea level
DEM	Digital Elevation Model
Nunatak	exposed pinnacle of rock surrounding by thick ice
exposure age	the time since material has been uncovered
ice rise	a dome of ice with higher elevation and slower flow speed than surrounding ice
RFIS	Ronne Filchner Ice Shelf

Data Availability Statement

Ground-based ice-penetrating radar data can be obtained from the UK Polar Data Center (http://doi.org/99d). A MATLAB script for viewing the raw radar data is also provided at this link. The digital elevation model of the SWSE, and radar data used to build it, are available at (https://doi.org/10.5194/essd-10-711-2018).

Acknowledgments

We thank David Small for drafting Figure 8. Funding was provided by the UK Natural Environment Research Council to M. J. S. (NE/G013071/1), S. S. R. J. (NE/R000824/1), D. E. S. (NE/1025840/1), J. W. (NE/I027576/1), and M. J. B. (NE/F014260/1, NE/J008176/1, and NE/K003674/1).

References

Anandakrishnan, S., & Alley, R. B. (1997). Stagnation of ice stream C, West Antarctica by water piracy. *Geophysical Research Letters*, *24*, 265–268.

Argus, D. F., Peltier, W. R., Drummond, R., & Moore, A. W. (2014). The Antarctica component of postglacial rebound model ICE-6G_C (VM5a) based on GPS positioning, exposure age dating of ice thicknesses, and relative sea level histories. *Geophysical Journal International*, *198*, 537–563.

Arthern, R. J., Winebrenner, D. P., & Vaughan, D. G. (2006). Antarctic snow accumulation mapped using polarization of 4.3-cm wavelength microwave emission. *Journal of Geophysical Research*, *111*, D06107. https://doi.org/10.1029/2004JD005667

Asay-Davis, X. S., Cornford, S. L., Durand, G., Galton-Fenzi, B. K., Gladstone, R. M., Gudmundsson, G. H., et al. (2016). Experimental design for three interrelated marine ice sheet and ocean model intercomparison projects: MISMIP v. 3 (MISMIP +), ISOMIP v. 2 (ISOMIP +) and MISOMIP v. 1 (MISOMIP1). *Geoscientific Model Development*, *9*, 2471–2497. https://doi.org/10.5194/gmd-9-2471-2016

Balco, G. (2011). Contributions and unrealized potential contributions of cosmogenic-nuclide exposure dating to glacier chronology 1990–2010. *Quaternary Science Reviews*, *30*(1–2), 3–27.

Balco, G., Todd, C., Huybers, K., Campbell, S., Vermeulen, M., Hegland, M., et al. (2016). Cosmogenic-nuclide exposure ages from the Pensacola Mountains adjacent to the Foundation Ice Stream, Antarctica. *American Journal of Science*, *316*(6), 542–577.

Bamber, J. L., Vaughan, D. G., & Joughin, I. (2000). Widespread complex flow in the interior of the Antarctic ice sheet. *Science*, *287*(5456), 1248–1250. https://doi.org/10.1126/science.287.5456.1248

Bell, R. E., Ferraccioli, F., Creyts, T. T., Braaten, D., Corr, H., Das, I., et al. (2011). Widespread persistent thickening of the East Antarctic ice sheet by freezing from the base. *Science*, *331*, 1592–1595. https://doi.org/10.1126/science.1200109

Bentley, M. J., Fogwill, C. J., Le Brocq, A. M., Hubbard, A. L., Sugden, D. E., Dunai, T., & Freeman, S. P. H. T. (2011). Deglacial history of the West Antarctic ice sheet in the Weddell Sea embayment: Constraints on past ice volume change: REPLY. *Geology*, *39*, e240. https://doi.org/10.1130/G32140Y.1

Bentley, M. J., Fogwill, C. J., Le Brocq, A. M., Hubbard, A. L., Sugden, D. E., Dunai, T. J., & Freeman, S. P. H. T. (2010). Deglacial history of the West Antarctic ice sheet in the Weddell Sea embayment: constraints on past ice volume and change. *Geology*, *38*, 411–414. https://doi.org/10.1130/G30754.1.

Bentley, M. J., Hein, A. S., Sugden, D. E., Whitehouse, P. L., Shanks, R., Xu, S., & Freeman, S. P. H. T. (2017). Deglacial history of the Pensacola Mountains, Antarctica from glacial geomorphology and cosmogenic nuclide surface exposure dating. *Quaternary Science Reviews*, *158*, 58–76.

Bentley, M. J., Ó Cofaigh, C., Anderson, J. B., Conway, H., Davies, B., Graham, A. G. C., et al. (2014). A community-based geological reconstruction of Antarctic ice sheet deglaciation since the Last Glacial Maximum. *Quaternary Science Reviews*, *100*, 1–9.

Bindschadler, R. A., Vaughan, D. G., & Vornberger, P. (2011). Variability of basal melt beneath the Pine Island Glacier ice shelf, West Antarctica. *Journal of Glaciology*, *57*(204), 581–595. https://doi.org/10.3189/002214311797409802

Bindschadler, R. A., Vornberger, P., Flemming, A., Fox, A., Mullins, J., Binnie, D., et al. (2008). The Landsat image mosaic of Antarctica. *Remote Sensing of the Environment*, *112*, 4214–4226. https://doi.org/10.1016/j.rse.2008.07.006

Bingham, R., & Siegert, M. J. (2007). Radio-echo sounding over polar ice masses. *Journal of Environmental & Engineering Geophysics*, *12*, 47–62.

Bingham, R. G., Siegert, M. J., Blankenship, D. D., & Young, D. A. (2007). Organized flow from the South Pole to the Filchner-Ronne ice shelf: An assessment of balance velocities in interior East Antarctica using radio-echo sounding data. *Journal of Geophysical Research*, *112*, F03S26. https://doi.org/10.1029/2006JF000556.

Bons, P. D., Jansen, D., Mundel, F., Bauer, C. C., Binder, T., Eisen, O., et al. (2016). Converging flow and anisotrophy cause large-scale folding in Greenland's ice sheet. *Nature Communications*, *7*, 11427. https://doi.org/10.1038/ncomms11427

Bradley, S. L., Hindmarsh, R. C. A., Whitehouse, P. L., Bentley, M. J., & King, M. A. (2015). Low post-glacial rebound rates in the Weddell Sea due to Late Holocene ice-sheet readvance. *Earth and Planetary Science Letters*, *414*, 79–79. https://doi.org/10.1016/j.epsl.2014.12.039

Briggs, R. D., Pollard, D., & Tarasov, L. (2014). A data-constrained large ensemble analysis of Antarctic evolution since the Eemian. *Quaternary Science Reviews*, *103*, 91–115.

Brisbourne, A. M., Martín, C., Smith, A. M., Baird, A. F., Kendall, J. M., & Kingslake, J. (2019). Constraining recent ice flow history at Korff Ice Rise, West Antarctica, using radar and seismic measurements of ice fabric. *Journal of Geophysical Research: Earth Surface*, *124*, 175–194. https://doi.org/10.1029/2018JF004776

Brunt, K. E., Fricker, H. A., & Padman, L. (2011). Analysis of ice plains of the Filchner-Ronne Ice Shelf, Antarctica, using ICESat laser altimetry. *Journal of Glaciology*, *57*, 965–975.

Bueler, E., Lingle, C., & Brown, J. (2007). Fast computation of a viscoelastic deformable Earth model for ice-sheet simulations. *Annals of Glaciology*, *46*, 97–105.

Catania, G. A., Scambos, T. A., Conway, H., & Raymond, C. F. (2006). Sequential stagnation of Kamb Ice Stream, West Antarctica. *Geophysical Research Letters*, *33*, L14502. https://doi.org/10.1029/2006GL026430

Catania, G. A., Scambos, T. A., Conway, H., & Raymond, C. F. (2012). Sequential stagnation of Kamb Ice Stream, West Antarctica. *Journal of Glaciology*, *58*(210). https://doi.org/10.3189/2012JoG11J219. (2012).

Clark, P. U. (2011). Deglacial history of the West Antarctic ice sheet in the Weddell Sea embayment: Constraints on past ice volume change: Comment. *Geology*. https://doi.org/10.1130/G31533C.1

Conway, H., Hall, B. L., Denton, G. H., Gades, A. M., & Waddington, E. D. (1999). Past and future grounding-line retreat of the West Antarctic Ice Sheet. *Science*, *286*, 280–283.

Cornford, S. L., Martin, D. F., Payne, A. J., Ng, E. G., Le Brocq, A. M., Gladstone, R. M., et al. (2015). Century-scale simulations of the response of the West Antarctic Ice Sheet to a warming climate. *Cryosphere*, *9*, 1579–1600. https://doi.org/10.5194/tc-9-1579-2015

Curtis, M. L. (2001). Tectonic history of the Ellsworth Mountains, West Antarctica: Reconciling a Gondwana enigma. *Geological Society of America Bulletin*, *113*, 939–958.

Dalziel, I. W. D., & Elliot, D. H. (1982). West Antarctica: Problem child of Gondwanaland. *Tectonics*, *1*, 3–19. https://doi.org/10.1029/TC001i001p00003

de Boer, B., Stocchi, P., Whitehouse, P. L., & van de Wal, R. S. W. (2017). Current state and future perspectives on coupled ice-sheet–sea-level modelling. *Quaternary Science Reviews*, *169*, 13–28. https://doi.org/10.1016/j.quascirev.2017.05.013

Dowdeswell, J. A., & Evans, S. (2004). Investigations of the form and flow of ice sheets and glaciers using radio-echo sounding. *Reports on Progress in Physics*, *67*, 1821–1861.

Engels, O., Gunter, B. C., Riva, R. E. M., & Klees, R. (2018). Separating geophysical signals using GRACE and high-resolution data: A case study in Antarctica. *Geophysical Research Letters*, *45*, 12,340–12,349.
Favier, L., & Pattyn, F. (2015). Antarctic ice rise formation, evolution, and stability. *Geophysical Research Letters*, *42*, 4456–4463. https://doi.org/10.1002/2015GL064195
Fretwell, P., Pritchard, H. D., Vaughan, D. G., Bamber, J. L., Barrand, N. E., Bell, R., et al. (2013). Bedmap2: Improved ice bed, surface and thickness datasets for Antarctica. *The Cryosphere*, *7*(1), 375–393. https://doi.org/10.5194/tc-7-375-2013
Geruo, A., Wahr, J., & Zhong, S. J. (2013). Computations of the viscoelastic response of a 3-D compressible Earth to surface loading: An application to Glacial Isostatic Adjustment in Antarctica and Canada. *Geophysical Journal International*, *192*, 557–572.
Goehring, B. M., Balco, G., Todd, C., Moening-Swanson, I., & Nichols, K. (2019). Late-glacial grounding line retreat in the northern Ross Sea, Antarctica. *Geology*, *47*, 291–294. https://doi.org/10.1130/G45413.1
Goehring, B. M., Schaefer, J. M., Schluechter, C., Lifton, N. A., Finkel, R. C., Jull, A. J. T., et al. (2011). The Rhone Glacier was smaller than today for most of the Holocene. *Geology*, *39*(7), 679–682.
Golledge, N. R., Menviel, L., Carter, L., Fogwill, C. J., England, M. H., Cortese, G., & Levy, R. H. (2014). Antarctic contribution to meltwater pulse 1A from reduced Southern Ocean overturning. *Nature Communications*, *5*(1). https://doi.org/10.1038/ncomms6107
Gomez, N., Latychev, K., & Pollard, D. (2018). A coupled ice sheet-sea level model incorporating 3D Earth structure: Variations in Antarctica during the last deglacial retreat. *Journal of Climate*, *31*, 4041–4054.
Gomez, N., Mitrovica, J. X., Huybers, P., & Clark, P. U. (2010). Sea level as a stabilizing factor for marine-ice-sheet grounding lines. *Nature Geoscience*, *3*, 850–853.
Gomez, N., Pollard, D., & Holland, D. (2015). Sea-level feedback lowers projections of future Antarctic Ice-Sheet mass loss. *Nature Communications*, *6*(1), 8798. https://doi.org/10.1038/ncomms9798
Gomez, N., Pollard, D., & Mitrovica, J. X. (2013). A 3-D coupled ice sheet-sea level model applied to Antarctica through the last 40 ky. *Earth and Planetary Science Letters*, *384*, 88–99.
Gunter, B. C., Didova, O., Riva, R. E. M., Ligtenberg, S. R. M., Lenaerts, J. T. M., King, M. A., et al. (2014). Empirical estimation of present-day Antarctic glacial isostatic adjustment and ice mass change. *The Cryosphere*, *8*(2), 743–760. https://doi.org/10.5194/tc-8-743-2014
Haran, T., J. Bohlander, T. Scambos, T. Painter, and M. Fahnestock. MODIS Mosaic of Antarctica 2003–2004 (MOA2004) Image Map. [indicate subset used]. Boulder, Colorado USA: National Snow and Ice Data Center. https://doi.org/10.7265/N5ZK5DM5 (2005)
Hay, C. C., Lau, H. C. P., Gomez, N., Austermann, J., Powell, E., Mitrovica, J. X., et al. (2017). Sea-level fingerprints in a region of complex Earth structure: the case of WAIS. *Journal of Climate*, *30*(6), 1881–1892. https://doi.org/10.1175/JCLI-D-16-0388.1
Hein, A. S., Fogwill, C. J., Sugden, D. E. & Xu, S. (2014). Geological scatter of cosmogenic-nuclide exposure ages in the Shackleton Range, Antarctica:Implications for glacial history. *Quaternary Geochronology*. *19*, 52–66. https://doi.org/10.1016/j.quageo.2013.03.008
Hein, A. S., Marrero, S. M., Woodward, J., Dunning, S. A., Winter, K., Westoby, M. J., et al. (2016). Mid-Holocene pulse of thinning in the Weddell Sea sector of the West Antarctic ice sheet. *Nature Communications*, *7*(1). https://doi.org/10.1038/ncomms12511
Hein, A. S., Fogwill, C. J., Sugden, D. E. & Xu, S. (2011). Glacial/interglacial ice-stream stability in the Weddell Sea embayment, Antarctica. *Earth and Planetary Science Letters*, *307*, 211–221. https://doi.org/10.1016/j.epsl
Hein, A. S., Woodward, J., Marrero, S. M., Dunning, S. A., Steig, E. J., Freeman, S. P. H. T., et al. (2016). Evidence of the stability of the West Antarctic Ice Sheet divide for 1.4 million years. *Nature Communications*, *7*(1).
Hellmer, H. H., Kauker, F., Timmermann, R., Determann, J., & Rae, J. (2012). Twenty-first-century warming of a large Antarctic ice-shelf cavity by a redirected coastal current. *Nature*, *485*, 225–228.
Hillenbrand, C. D., Bentley, M. J., Stolldorf, T. D., Hein, A. S., Kuhne, G., Graham, A. G. C., et al. (2014). *Quaternary Science Reviews*, *100*, 111–136.
Holschuh, N., Christianson, K., Conway, H., Jacobel, R. W., & Welch, B. C. (2018). Persistent tracers of historic ice flow in glacial stratigraphy near Kamb Ice Stream, West Antarctica. *The Cryosphere*, *12*, 2821–2829. https://doi.org/10.5194/tc-12-2821-2018
Intergovernmental Panel on Climate Change (2013). In T. F. Stocker, D. Qin, G.-K. Plattner, M. Tignor, S. K. Allen, J. Boschung, A. Nauels, Y. Xia, V. Bex, & P. M. Midgley (Eds.), *Climate Change 2013: The physical science basis. Contribution of Working Group I to the Fifth Assessment Report of the Intergovernmental Panel on Climate Change*, (p. 1535). Cambridge, United Kingdom and New York, NY, USA: Cambridge University Press.
Ivins, E. R., James, T. S., Wahr, J., O. Schrama, E. J., Landerer, F. W., & Simon, K. M. (2013). Antarctic contribution to sea-level rise observed by GRACE with improved GIA correction. *Journal of Geophysical Research: Solid Earth*, *118*, 3126–3141. https://doi.org/10.1002/jgrb.50208
Jeofry, H., Ross, N., Corr, H. F. J., Li, J., Morlighem, M., Gogineni, P., & Siegert, M. J. (2018). A new digital elevation model for the Weddell Sea sector of the West Antarctic Ice Sheet. *Earth System Science Data*, *10*, 711–725. https://doi.org/10.5194/essd-10-711-2018
Jeofry, H., Ross, N., Le Brocq, A., Graham, A., Li, J., Gogineni, P., et al. (2018). Hard rock landforms generate 130 km ice shelf channels through water focusing in basal corrugations. *Nature Communications*, *9*, 4576. https://doi.org/10.1038/s41467-018-06679-z
Johnson, J. S., Nichols, K. A., Goehring, B. M., Balco, G., & Schaefer, J. M. (2019). Abrupt mid-Holocene ice loss in the western Weddell Sea Embayment of Antarctica. *Earth and Planetary Science Letters*, *518*, 127–135. https://doi.org/10.1016/j.epsl.2019.05.002
Jones, R. S., Mackintosh, A. N., Norton, K. P., Golledge, N. R., Fogwill, C. J., Kubik, P. W., et al. (2015). Rapid Holocene thinning of an East Antarctic outlet glacier driven by marine ice sheet instability. *Nature communications 6*, p. 8910. https://doi.org/10.1038/ncomms9910
Jordan, T. A., Ferraccioli, F., Ross, N., Corr, H. F. J., Leat, P. T., Bingham, R. G., et al. (2013). Inland extent of the Weddell Sea Rift imaged by new aerogeophysical data. *Tectonophysics*, *585*, 137–160. https://doi.org/10.1016/j.tecto.2012.09.010
Jordan, T. A., Martin, C., Ferraccioli, F., Matsuoka, K., Corr, H., Forsberg, R., et al. (2018). Geothermal anomaly facilitates ice-flow variability in East Antarctic Ice Sheet interior. *Scientific Reports*, *8*, 16785. https://doi.org/10.1038/s41598-018-35182-0(2018)
Joughin, I., Smith, B. E., & Medley, B. (2014). Marine ice sheet collapse potentially under way for the Thwaites Glacier Basin, West Antarctica. *Science*, *344*, 735–738. https://doi.org/10.1126/science.1249055
Kingslake, J., Martín, C., Arthern, R. J., Corr, H. F. J., & King, E. C. (2016). Ice-flow reorganization in West Antarctica 2.5 kyr ago dated using radar-derived englacial flow velocities. *Geophysical Research Letters*, *43*, 9103–9112. https://doi.org/10.1002/2016GL070278
Kingslake, J., Scherer, R. P., Albrecht, T., Coenen, J., Powell, R. D., Reese, R., et al. (2018). Extensive retreat and re-advance of the West Antarctic ice sheet during the Holocene. *Nature*, *558*(7710), 430.
Konrad, H., Sasgen, I., Pollard, D., & Klemann, V. (2015). Potential of the solid-Earth response for limiting long-term West Antarctic Ice Sheet retreat in a warming climate. *Earth and Planetary Science Letters*, *432*, 254–264.
Lal, D. (1991). Cosmic-ray labelling of erosion surfaces—In situ nuclide production-rates and erosion models. *Earth and Planetary Science Letters*, *104*(2–4), 424–439.

Le Brocq, A., Ross, N., Griggs, J., Bingham, R., Corr, H., Ferroccioli, F., et al. (2013). Ice shelves record the history of channelised flow beneath the Antarctic ice sheet. *Nature Geoscience*, *6*, 945–948. https://doi.org/10.1038/ngeo1977.

Le Brocq, A. M., Bentley, M. J., Hubbard, A., Fogwill, C. J., Sugden, D. E., & Whitehouse, P. L. (2011). Reconstructing the Last Glacial Maximum ice sheet in the Weddell Sea embayment, Antarctica, using numerical modelling constrained by field evidence. *Quaternary Science Reviews*, *30*, 2422–2432. https://doi.org/10.1016/j.quascirev.2011.05.009

Mackintosh, A., White, D., Fink, D., Gore, D. B., Pickard, J., & Fanning, P. C. (2007). Exposure ages from mountain dipsticks in Mac. Robertson Land, East Antarctica, indicate little change in ice-sheet thickness since the Last Glacial Maximum. *Geology*, *35*(6), 551–554.

Maris, M. N. A., de Boer, B., Ligtenberg, S. R. M., Crucifix, M., van de Berg, W. J., & Oerlemans, J. (2014). Modelling the evolution of the Antarctic ice sheet since the last interglacial. *The Cryosphere*, *8*, 1347–1360. https://doi.org/10.5194/tc-8-1347-2014

Martín, C., Hindmarsh, R. C. A., & Navarro, F. J. (2006). Dating ice flow change near the flow divide at Roosevelt Island, Antarctica, by using a thermomechanical model to predict radar stratigraphy. *Journal of Geophysical Research*, *111*, F01011. https://doi.org/10.1029/2005JF000326

Martín, C., Hindmarsh, R. C. A., & Navarro, F. J. (2009). On the effects of divide migration, along-ridge flow, and basal sliding on isochrones near an ice divide. *Journal of Geophysical Research*, *114*, F02006. https://doi.org/10.1029/2008JF001025.

Martín-Español, A., King, M. A., Zammit-Mangion, A., Andrews, S. B., Moore, P., & Bamber, J. L. (2016). An assessment of forward and inverse GIA solutions for Antarctica. *Journal of Geophysical Research: Solid Earth*, *121*, 6947–6965. https://doi.org/10.1002/2016JB013154

Martín-Español, A., Zammit-Mangion, A., Clarke, P. J., Flament, T., Helm, V., King, M. A., et al. (2016). Spatial and temporal Antarctic Ice Sheet mass trends, glacio-isostatic adjustment, and surface processes from a joint inversion of satellite altimeter, gravity, and GPS data. *Journal of Geophysical Research: Earth Surface*, *121*, 182–200. https://doi.org/10.1002/2015JF003550

Matsuoka, K., Hindmarsh, R. C. A., Moholdt, G., Bentley, M. J., Pritchard, H. D., Brown, J., et al. (2015). Antarctic ice rises and rumples: their properties and significance for ice-sheet dynamics and evolution. *Earth-Science Reviews*, *150*, 724–745. https://doi.org/10.1016/j.earscirev.2015.09.004

McConnell, R. K. (1965). Isostatic adjustment in a layered Earth. *Journal of Geophysical Research*, *70*. https://doi.org/10.1029/JZ070i020p05171

Mitrovica, J., & Forte, A. (2004). A new inference of mantle viscosity based upon joint inversion of convection and glacial isostatic adjustment data. *Earth and Planetary Science Letters*, *225*, 177–189.

Morse, D. L., Waddington, E. D., & Steig, E. J. (1998). Ice age storm trajectories inferred from radar stratigraphy at Taylor Dome, Antarctica. *Geophysical Research Letters*, *25*(17), 3383–3386.

Mouginot, J., Rignot, E., Scheuchl, B., & Millan, R. (2017). Comprehensive annual ice sheet velocity mapping using Landsat-8, Sentinel-1, and RADARSAT-2 data. *Remote Sensing*, *9*, 364–1370.

Mulvaney, R., Oerter, H., Peel, D. A., Graf, W., Arrowsmith, C., Pasteur, E. C., et al. (2002). 1000-year ice core records from Berkner Island, Antarctic. *Annals of Glaciology*, *35*, 45–51. https://doi.org/10.3189/172756402781817176

Nichols, K. A., Goehring, B. M., Balco, G., Johnson, J. S., Hein, A. A., & Todd, C. (2019). New Last Glacial Maximum Ice Thickness constraints for the Weddell Sea sector, Antarctica. *The Cryosphere Discuss*. https://doi.org/10.5194/tc-2019-64

Nield, G. A., Whitehouse, P. L., van der Wal, B., Blank, B., O'Donnell, P., & Stuart, G. W. (2018). The impact of lateral variations in lithospheric thickness on glacial isostatic adjustment in West Antarctica. *Geophysical Journal International*, (2), 811–824. https://doi.org/10.1093/gji/ggy158

Pollard, D., Gomez, N., & DeConto, R. M. (2017). Variations of the Antarctic ice sheet in a coupled ice sheet-Earth-sea level model: sensitivity to viscoelastic Earth properties. *Journal of Geophysical Research: Earth Surface*, *122*, 2124–2138. https://doi.org/10.1002/2017JF004371

Raymond, C. F. (1983). Deformation in the vicinity of ice divides. *Journal of Glaciology*, *29*, 357–373.

Rignot, E., Mouginot, J., & Scheuchl, B. (2011). MEaSUREs InSAR-based Antarctica ice velocity map, version 2, Boulder, Colorado USA, NASA National Snow and Ice Data Center Distributed Active Archive Center. https://doi.org/10.5067/D7GK8F5J8M8R

Rignot, E., Mouginot, J., Scheuchl, B., van den Broeke, M., van Wessem, M. J., & Morlighem, M. (2018). Four decades of Antarctic Ice Sheet mass balance from 1979–2017. *Proceedings of the National Academy of Sciences*, *116*, 1095–1103. https://doi.org/10.1073/pnas.1812883116

Rose, K. C., Ross, N., Bingham, R. G., Corr, H. F. J., Ferraccioli, F., Jordan, T. A., et al. (2014). A temperate former West Antarctic ice sheet suggested by an extensive zone of bed channels. *Geology*, *42*, 971–974. https://doi.org/10.1130/G35980.1

Rose, K. C., Ross, N., Jordan, T. A., Bingham, R. G., Corr, H., Ferraccioli, F., et al. (2015). Ancient pre-glacial erosion surfaces preserved beneath the West Antarctic ice sheet. *Earth Surface Dynamics*, *3*, 139–152. https://doi.org/10.5194/esurf-3-139-2015

Rosier, S. H. R., Hofstede, C., Brisbourne, A. M., Hattermann, R., Nicholls, K. W., Davis, P. E. D., et al. (2018). A new bathymetry for the southeastern Filchner-Ronne Ice Shelf: Implications for modern oceanographic processes and glacial history. *Journal of Geophysical Research: Oceans*, *123*, 4610–4623. https://doi.org/10.1029/2018JC013982

Ross, N., Bingham, R. G., Corr, H., Ferraccioli, F., Jordan, T. A., Le Brocq, A., et al. (2012). Steep reverse bed slope at the grounding line of the Weddell Sea sector in West Antarctica. *Nature Geoscience*, *5*, 393–396. https://doi.org/10.1038/ngeo1468

Ross, N., Jordan, T. A., Bingham, R. G., Corr, H. F. J., Ferraccioli, F., Le Brocq, A., et al. (2014). The Ellsworth Subglacial Highlands: Inception and retreat of the West Antarctic Ice Sheet. *Geological Society of America Bulletin*, *126*, 3–15. https://doi.org/10.1130/B30794.1

Ross, N., & Siegert, M. (2014). Concentrated englacial shear over rigid basal ice, West Antarctica: Implications for modeling and ice sheet flow. *Geophysical Research Abstracts*, *16*, EGU2014–EGU5568.

Ross, N., Siegert, M. J., Woodward, J., Smith, A. M., Corr, H. F. J., Bentley, M. J., et al. (2011). Holocene stability of the Pine Island Glacier-Weddell Sea ice divide, West Antarctica. *Geology*, *39*(10), 935–938.

Sasgen, I., Martín-Español, A., Horvath, A., Klemann, V., Petrie, E. J., Wouters, B., et al. (2017). Joint inversion estimate of regional glacial isostatic adjustment in Antarctica considering a lateral varying Earth structure (ESA STSE Project REGINA). *Geophysical Journal International*, *211*(3), 1534–1553. https://doi.org/10.1093/gji/ggx368

Scambos, T., Haran, T., Fahnestock, M., Painter, T., & Bohlander, J. (2007). MODIS-based Mosaic of Antarctica (MOA) Data Sets: Continent-wide surface morphology and snow grain size. *Remote Sensing of Environment*, *111*(2), 242–257. https://doi.org/10.1016/j.rse.2006.12.020

Shen, W., Wiens, D. A., Anandakrishnan, S., Aster, R. C., Gerstoft, P., Bromirski, P. D., et al. (2018). The crust and upper mantle structure of central and West Antarctica from Bayesian inversion of Rayleigh wave and receiver functions. *Journal of Geophysical Research: Solid Earth*, *123*, 7824–7849. https://doi.org/10.1029/2017JB015346

Shepherd, A. (2018). Mass balance of the Antarctic ice sheet from 1992 to 2017. *Nature*, *558*(7709), 219–222. https://doi.org/10.1038/s41586-018-0179-y

Siegert, M. J. (1999). On the origin, nature and uses of Antarctic ice-sheet radio-echo layering. *Progress in Physical Geography*, *23*, 159–179.

Siegert, M. J. (2001). *Ice sheets and Late Quaternary environmental change* (p. 231). Chichester, UK: John Wiley.

Siegert, M. J., Clarke, R. J., Mowlem, M., Ross, N., Hill, C. S., Tait, A., et al. (2012). Clean access, measurement and sampling of Ellsworth Subglacial Lake: A method to explore deep Antarctic subglacial lake environments. *Reviews of Geophysics*, *50*, RG1003. https://doi.org/10.1029/2011RG000361

Siegert, M. J., & Leysinger Vieli, G. J. M. C. (2007). Late glacial history of the Ross Sea sector of the West Antarctic ice sheet: Evidence from englacial layering at Talos Dome, East Antarctica. *Journal of Environmental and Engineering Geophysics*, *12*, 63–67.

Siegert, M. J., & Payne, A. J. (2004). Past rates of accumulation in central West Antarctica. *Geophysical Research Letters*, *31*, L12403. https://doi.org/10.1029/2004GL020290

Siegert, M. J., Ross, N., Corr, H., Kingslake, J., & Hindmarsh, R. (2013). Late Holocene ice-flow reconfiguration in the Weddell Sea sector of West Antarctica. *Quaternary Science Reviews*, *78*, 98–107. https://doi.org/10.1016/j.quascirev.2013.08.003

Siegert, M. J., Ross, N., Li, J., Schroeder, D., Rippin, D., Ashmore, D., et al. (2016). Controls on the onset and flow of Institute Ice Stream, West Antarctica. *Annals of Glaciology*, *57*, 19–24. https://doi.org/10.1017/aog.2016.17

Siegert, M. J., Welch, B., Morse, D., Vieli, A., Blankenship, D. D., Joughin, I., et al. (2004). Ice flow direction change in interior West Antarctica. *Science*, *305*, 1948–1951. https://doi.org/10.1126/science.1101072

Smith, B. E., Fricker, H. A., Joughin, I. R., & Tulaczyk, S. (2009). An inventory of active subglacial lakes in Antarctica detected by ICESat (2003–2008). *Journal of Glaciology*, *55*(129), 573–595.

Stone, J. O., Balco, G. A., Sugden, D. E., Caffee, M. W., Sass, L. C., Cowdery, S. G., & Siddoway, C. (2003). Holocene deglaciation of Marie Byrd Land, West Antarctica. *Science*, *299*(5603), 99–102.

Sugden, D. E., Hein, A. S., Woodward, J., Marrero, S. M., Rodés, A., Dunning, S. A., et al. (2017). The million-year evolution of the glacial trimline in the southernmost Ellsworth Mountains, Antarctica. *Earth and Planetary Science Letters*, *469*, 42–52. https://doi.org/10.1016/j.epsl.2017.04.006

Sugden, D. E., & Jamieson, S. S. R. (2018). The pre-glacial landscape of Antarctica. *Scottish Geographical Journal*, *134*(3-4), 203–223. https://doi.org/10.1080/14702541.2018.1535090

van der Wal, W., Whitehouse, P. L., & Schrama, E. J. O. (2015). Effect of GIA models with 3D composite mantle viscosity on GRACE mass balance estimates for Antarctica. *Earth and Planetary Science Letters*, *414*, 134–143.

van Wessem, J. M., Jan Van De Berg, W., Noël, B. P., Van Meijgaard, E., Amory, C., Birnbaum, G., et al. (2018). Modelling the climate and surface mass balance of polar ice sheets using RACMO2: Part 2: Antarctica (1979-2016). *The Cryosphere*, *12*(4), 1479–1498.

W.A.I.S. Drilling Project Members (2013). Onset of deglacial warming in West Antarctica driven by local orbital forcing. *Nature*, *500*, 440–444.

White, D., Fulop, R. H., Bishop, P., Mackintosh, A., & Cook, G. (2011). Can in-situ cosmogenic C-14 be used to assess the influence of clast recycling on exposure dating of ice retreat in Antarctica? *Quaternary Geochronology*, *6*(3–4), 289–294.

Wearing, M. G., & Kingslake, J. (2019). Holocene Formation of Henry Ice Rise, West Antarctica, Inferred from Ice-Penetrating Radar. *Journal of Geophysical Research: Earth Surface*. *124*, 8, 2224–2240. https://doi.org/10.1029/2018JF004988

Whitehouse, P. L. (2018). Glacial isostatic adjustment modelling: historical perspectives, recent advances, and future directions. *Earth Surface Dynamics*, *6*, 401–429.

Whitehouse, P. L., Bentley, M. J., & Le Brocq, A. M. (2012). A deglacial model for Antarctica: Geological constraints and glaciological modelling as a basis for a new model of Antarctic glacial isostatic adjustment. *Quaternary Science Reviews*, *32*, 1–24.

Whitehouse, P. L., Bentley, M. J., Milne, G. A., King, M. A., & Thomas, I. D. (2012). A new glacial isostatic adjustment model for Antarctica: calibrated and tested using observations of relative sea-level change and present-day uplift rates. *Geophysical Journal International*, *190*, 1464–1482. https://doi.org/10.1111/j.1365-246X.2012.05557.x

Whitehouse, P. L., Bentley, M. J., Vieli, A., Jamieson, S. S. R., Hein, A. S., & Sugden, D. E. (2017). Controls on Last Glacial Maximum ice extent in the Weddell Sea embayment, Antarctica. *Journal of Geophysical Research: Earth Surface*, *122*, 371–397. https://doi.org/10.1002/2016JF004121

Whitehouse, P. L., Gomez, N., King, M. A., & Wiens, D. A. (2019). Solid Earth change and the evolution of the Antarctic Ice Sheet. *Nature Communications*, *10*, 503.

Winter, K., Ross, N., Ferraccioli, F., Jordan, T., Corr, H. F. J., Forsberg, R., et al. (2018). Topographic steering of enhanced ice flow at the bottleneck between East and West Antarctica. *Geophysical Research Letters*, *45*, 4899–4907. https://doi.org/10.1029/2018GL077504

Winter, K., Woodward, J., Dunning, S. A., Turney, C. S. M., Fogwill, C. J., Hein, A. S., et al. (2016). Assessing the continuity of the blue ice climate record at Patriot Hills, Horseshoe Valley, West Antarctica. *Geophysical Research Letters*, *43*, 2019–2026. https://doi.org/10.1002/2015GL066476

Winter, K., Woodward, J., Ross, N., Dunning, S. A., Corr, H. F. J., Bingham, R. J., & Siegert, M. J. (2015). Airborne radar evidence for tributary flow switching in the Institute Ice Stream upper catchment, West Antarctica: Implications for ice sheet configuration and dynamics. *Journal of Geophysical Research: Earth Surface*, *120*, 1611–1625. https://doi.org/10.1002/2015JF003518

Winter, K., Woodward, J., Ross, N., Dunning, S. A., Hein, A. S., Westoby, M. J., et al. (2019). Radar-detected englacial debris in the West Antarctic Ice Sheet. *Geophysical Research Letters*, *46*. https://doi.org/10.1029/2019GL084012

Wolovick, M. J., Creyts, T. T., Buck, W. R., & Bell, R. E. (2014). Traveling slippery patches produce thickness-scale folds in ice sheets. *Geophysics Research Letters*, *41*, 8895–8901. https://doi.org/10.1002/2014GL062248

Wolstencroft, M., King, M. A., Whitehouse, P. L., Bentley, M. J., Nield, G. A., King, E. C., et al. (2015). Uplift rates from a new high-density GPS network in Palmer Land indicate significant late Holocene ice loss in the southwestern Weddell Sea. *Geophysical Journal International*, *203*(1), 737–754. https://doi.org/10.1093/gji/ggv327

Woodward, J., Smith, A. M., Ross, N., Thoma, M., Corr, H. F. J., King, E. C., et al. (2010). Location for direct access to subglacial Lake Ellsworth. *Geophysical Research Letters*, *37*, L11501. https://doi.org/10.1029/2010GL042884.

Wright, A. P., Le Brocq, A. M., Cornford, S. L., Bingham, R. G., Corr, H. F. J., Ferroccioli, F., et al. (2014). Sensitivity of the Weddell Sea sector ice streams to sub-shelf melting and surface accumulation. *The Cryosphere*, *8*, 2119–2134. https://doi.org/10.5194/tc-8-2119-2014

Wright, A. P., & Siegert, M. J. (2012). A fourth inventory of Antarctic subglacial lakes. *Antarctic Science*, *24*, 659–664. https://doi.org/10.1017/S095410201200048X

Wrona, T., Wolovick, M., Ferraccioli, F., Corr, H., Jordan, T., & Siegert, M. J. (2018). Position and variability of complex structures in the central East Antarctic ice sheet. In M. J. Siegert, S. S. R. Jamieson, & D. A. White (Eds.), *Exploration of Subsurface Antarctica: Uncovering Past Changes and Modern Processes*, *Geological Society* (Vol. 461, pp. 113–130). London: Special Publications. https://doi.org/10.1144/SP461.12